The role of gas flushing on magma reservoir crystallization and its consequences for the growth of planetary crust

Bruno Scaillet

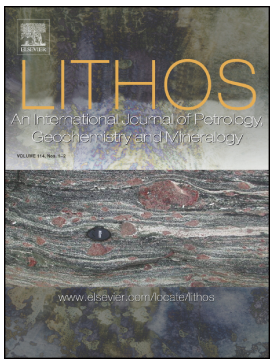

The role of gas flushing on magma reservoir crystallization and its consequences for the growth of planetary crust

Bruno Scaillet

PII: S0024-4937(22)00220-1

DOI: https://doi.org/10.1016/j.lithos.2022.106811

Reference: LITHOS 106811

To appear in: *LITHOS*

Received date: 26 January 2022

Revised date: 18 July 2022

Accepted date: 20 July 2022

Please cite this article as: B. Scaillet, The role of gas flushing on magma reservoir crystallization and its consequences for the growth of planetary crust, *LITHOS* (2022), https://doi.org/10.1016/j.lithos.2022.106811

The role of gas flushing on magma reservoir crystallization and its consequences for the growth of planetary crust

Bruno Scaillet

ISTO-UMR 7327 Université d'Orléans-CNRS-BRGM, 1a rue de la Férollerie, 45071 Orléans cedex 2, France

Corresponding author:bruno.scaillet@cnrs-orleans.fr

Abstract

Many crustal magmatic reservoirs are fundamentally powered by basalt injection at their base. Asides from transfer of silicate liquid and crystals and accompanying heat, basaltic magma also provides large amounts of fluids to the overlying magma. This work explores how water activity and temperature, hence degree of crystallisation, of magmatic reservoirs are affected by such a mechanism at various levels in the crust. By using recent experimental phase equilibria, thermodynamic relationships between gas and silicate melts, and heat balance, it is shown that, depending on the level of magma storage, diffusive exchange during bubble uprise and stalling may produce either crystallisation or melting of magmas. Long term fluxing of felsic to intermediate magma bodies stored in upper crust by mafic volatiles will generally lead to their near isothermal solidification. Conversely, for bodies stagnating in the mid to deep crust, such a process almost inevitably enhances melting, driving or maintaining magmas beyond the threshold of mobility needed for upward material transfer, unless the percolating fluid is very CO_2-rich. Compilation of basaltic melt inclusion data gathered in arc, hot-spot and ridge settings, shows that the two last categories coexist with CO_2-rich fluids at high pressures (XH_2O_{fluid}<0.1), which will almost always enhance crystallization. In contrast arc basalts record a wide and continuous range of fluid compositions, from dry to almost H_2O-saturated conditions, which may either favour (low pressure) or inhibit (high pressure) the crystallization of felsic reservoirs which they underplate. Crustal growth may thus be in part limited by the difficulty of crystallising deep-seated magma bodies, in particular in arc settings. This pressure controlled effect is related to the contrasted solubilities of H_2O and CO_2 in silicate melts, and to the much stronger non-ideal behaviour of CO_2 relative to H_2O as pressure increases. Asides from tectonic and density inversion processes, a thick crust may fundamentally reflect the fact that basalt underplating in the lower crust has proceeded at a rate sufficiently slow so as to prevent remelting of earlier intrusions (or melting of lower crust

lithologies) or that the outcoming fluid was CO_2-rich, or both. Application to other terrestrial planets is hindered by the paucity of data regarding crust thickness and composition, and it can be only conjectured that the thin crust of large planets (Earth, Venus) reflects in part the operation of subduction process during their evolution, while the comparatively thicker crust inferred for smaller bodies (Mars, the Moon, Vesta) reflects in turn processes related to a primordial crust.

INTRODUCTION

Magma underplating is an essential process on planets, being by virtue of progressive sill accumulation, the fundamental mechanism of crust production, be it basaltic or andesitic in composition. Upon crystallization, magmas lose their volatiles which may rise and percolate into overlying rocks, including former intrusions. Late intrusions may partially melt early ones (e.g., Bergantz, 1989) and give rise to differentiation processes (e.g., Hildreth and Morbath, 1988), in particular in the lower crust (e.g., Annen and Sparks, 2002; Dufek and Bergantz, 2005; Annen et al., 2006). In upper crust, gas percolation into silicic magmas from underlying crystallising basalt has been shown to affect in several ways the fluid mechanics of magma reservoirs, including density inversion leading to large scale overturn (e.g., Eichelberger, 1980 ; Huppert et al., 1982; Ruprecht et al., 2008), magma mixing (e.g., Thomas et al., 1993), inhibition of convection (Cardoso & Woods, 1999), filter pressing of residual liquids (Sisson & Bacon, 1999), or remelting due to advective heat transfer (e.g. Bachmann & Bergantz, 2005 ; Huber et al., 2010). However, whilst the physics of gas advection have been well studied (e.g., Parmigiani et al., 2014, 2016, 2017; Degruyter et al., 2019), little attention has been paid to evaluate the chemical effects of such a process. Yet, gas transfer from basalt is widely believed to be the ultimate source of volatiles in silicic magma bodies (e.g., Hattori, 1993 ; Wallace, 2005 ; Edmonds et al., 2010). The case for the transfer of CO_2-rich gas through shallow magma reservoirs in arc settings has been made previously (e.g., Blundy et al., 2010) and modelled in particular in the low pressure range (Yoshimura and Nakamura, 2011, 2013; Carrichi et al., 2018). These studies show that such a process may alter magma physical and chemical behaviour during or prior to eruption, leading in particular to enhanced crystallization of felsic magma reservoirs at rest, as expected from a thermodynamic viewpoint. Here I study the same process, but explore higher pressure

conditions and consider also the role of H_2O/CO_2 ratio of the injected fluid into the reservoir. I build upon recent phase equilibrium studies on a variety of magma compositions that constrain the combined effects of H_2O/CO_2 and temperature on magma crystallization up to 12 kbar, therefore encompassing the full range of common crust thickness, allowing insight into a pressure range where existing thermodynamic softwares, such as MELTs (e.g., Gualda et al., 2012), are not yet well calibrated, in particular because they miss important phases of hydrous magmas such as amphibole, which can be a preponderant crystallising phase at lower crustal conditions (e.g., Pichavant and Macdonald, 2007; Davidson et al., 2007). In the following I first present the conceptual framework related to bubble percolations through partly or fully molten magmas, and their expected effects of water activity. I then explore what happens when basaltic fluids (ie CO_2-richer as compared to those in more felsic magmas) ingress the magma reservoir, considering successively rhyolitic, dacitic, andesitic and basaltic compositions. The input fluid is considered to ingress the reservoir at a temperature not far from that of the stagnant felsic magma, which is an important assumption. The rationale for that stems from the following considerations: (1) on a long term basis, underplating is likely to proceed from the base of the felsic intrusion downwards (e.g., Annen and Burgisser, 2021). In such a situation, the fluid released by a newly arrived and crystallising mafic layer will percolate through the previous overlying intrusions which for the most part have come to thermal equilibrium with the felsic magma. This geometry will likely buffer the temperature of incoming fluids to that of the resident felsic body; (2) perhaps more importantly, the fundamental process of fluid addition from a mafic source, at least in arc systems, is due to the crystallization of the mafic end-member (e.g., Eichelberger, 1980; Huppert et al., 1982), i.e. its abrupt cooling resulting from its blending with the cold felsic magma, hence released mafic fluid will not be at the initial temperature of the mafic intrusion. It may well be however, that some mafic forerunners violate this geometry and arrive in the

upper reservoir while being still very hot: in such a circumstance, which is not explored in the present work, the excess heat brought by the hot fluid may counteract to some extent the CO_2-induced crystallization documented to occur at low pressure (see below). As concerns felsic magmas, the sole documented instance where this might occur is the Erebus system, whose permanent phonolitic lava lake is possibly sustained by continuous CO_2 flushing sourced from underlying basanitic magma (Oppenheimer et al., 2011).

An additional word of caution is needed at this point. In all calculations presented below, although no specific mention is made, nor is needed, for that the source of percolating fluids is assumed to be mafic, since basaltic magmatism is the fundamental process powering crustal growth or destruction (e.g. Hildreth, 1981). Yet, magma underplating processes need not to be exclusively represented by a mafic underneath silicic scenario, but could be also one in which an intermediate magma (ie andesite or dacite) encounters a more silicic one, or could be even that of a silicic injection into a more mafic reservoir (Eichelberger et al. 2000). These scenarios are not simulated here on the premise that the injection of a basalt into a silicic reservoir represents the commonest situation.

Expected crystallization/melting trends for felsic magmas underplated by basalts

To illustrate the chemical effects explored here, consider a reservoir at 2 kbar in which a partially crystallised magma is stored at 800°C with a melt water content of 5-6 wt% which corresponds to a mole fraction of water in the coexisting fluid phase, XH_2O_{fluid}, of 0.8 (A, Fig. 1). If such a reservoir is underplated by a basalt magma which supplies its volatiles upon crystallisation (e.g., Eichelberger, 1980; Huppert et al., 1982), four possibilities can occur (Fig. 1). The first case (A) is when the mafic gas has a composition (XH_2O_{fluid}) similar to that of the silicic host, in which case the influx of volatiles cannot alter the state of equilibrium and the system remains unchanged (ignoring heat contribution). The second case (B) is when

the mafic gas has a lower XH_2O_{fluid} than that of the resident magma, which forces the latter to crystallise (e.g., Carrichi et al., 2018). The third case (C), is the reverse of case B, ie the mafic gas composition is richer in H_2O than the resident one, and gas infiltration is accompagnied by remelting of the silicic mush. The fourth case (D) is when the mafic gas has an XH_2O_{fluid} equal to, or lower than, that of solidus. Excluding kinetics factors, the extent to which gas infiltration will alter the prevailing state of chemical equilibrium depends on the amount of gas supplied, the relationships between melt fraction and melt water content, and the contrast between the equilibrium fluid phase composition and that originated from the underlying basalt. Hydrothermal phase equilibria on magmas (e.g., Scaillet & Evans, 1999; Martel et al., 1999; Pichavant et al., 2002, Klimm et al., 2003) give the equilibrium relationship between melt fraction, melt H_2O content and fluid phase composition (Fig. 1), and from these works the general contours of wt% proportions of crystals in magmas can be drawn (Fig. 1). Below, I first briefly review some general considerations about the physics of bubble transfer through crystal mushes. For a detailed account on such a topic the reader is referred to Parmigiani et al. (2016) and references therein.

Bubble percolation in crystal mushes

The terminal ascent rate of bubbles in silicate melts can be calculated from Stokes'law:

$$V_s = (2\, r^2\, g\, \Delta d/9\, \mu).\, f(c) \qquad (1)$$

where r is the bubble radius, g the gravitational constant, Δd the density contrast and μ the viscosity of the melt. The term $f(c)$ is an empirical function that takes into account the effect of crystal content on ascent velocity (e.g., Bachmann and Bergantz, 2004) such that in a magma with 50% crystals the rising velocity is decreased by a factor of 10 relative to the crystal-free case. Application of the above equation to natural silicic to intermediate magmas in convergent settings is shown in Figure 2, using melt viscosities as constrained from phase

equilibrium data (Scaillet et al., 1998). The size distribution of bubbles in magma chambers is poorly known. Phase equilibrium experiments in which the silicate melt is equilibrated with H_2O-CO_2 bubbles show them to have radii in the range 10-100 microns, however, which is taken as a first order approximation for such a parameter. For such sizes, ascent rates in silicic reservoirs having 50% volume crystals are constrained to be on the order of a cm/y at best (Fig. 2). This value can be compared to the distance of volatile diffusion over the same duration. Both H_2O and CO_2 have diffusivities in the range 10^{-7}-$10^{-8}$$cm^2$/s for a rhyolite melt with 6-8 wt% dissolved H_2O at 800°C (e.g., Watson, 1994; Zhang et al., 2007). This yields a transport distance of about 1 cm/year, or a value similar to bubble ascent rates. Thus, although the above figures will vary depending on the specific case considered, they suggest that bubble migration through a partially molten magma is likely to proceed along with chemical exchange between gas and silicate melt, in particular when the percolated body is a crystal-rich magma with a viscous rhyolitic residual melt, since both factors act to decrease the ascent rate of bubbles.

Method of calculation

Calculations have been performed so as to find the final equilibrium fluid composition considering that the process is isenthalpic, since recent modelling has shown that heat advection via bubbles can lead to small but significant temperature increase (Bachmann & Bergantz, 2005; Carrichi et al., 2018). In most cases, amounts of fluid added up to 50 wt% have been considered which, though possibly unrealistic, constrain the limiting conditions towards which any system evolves for a given fluid composition. Considering that mafic arc magmas contain several wt% of H_2O (about 4 wt% Plank et al., 2013; Rasmussen et al., 2022), to > 6 wt% (e.g. Pichavant et al., 2002)), and possibly abundant CO_2 as well (e.g., Blundy et al., 2010; Plank and Manning, 2019), i.e. an amount of volatiles which is equivalent

to that inferred for felsic magmas, a supply of say 5-10 wt% fluid to a felsic body would require that the mass of mafic magma source of that fluid is broadly equal to that of the percolated silicic reservoir (see below). The case for other settings is less clear but there is growing evidence for enhanced fluid content of mafic magmas, in particular for those in hot-spot environments (several wt% as well, e.g., Dixon et al., 1997). The magma compositions used in this work, as well as the references corresponding to the studies having established the corresponding phase equilibria are listed in Table 1.

The following procedure was adopted :

For each composition at fixed pressure, the relationship between H_2O dissolved in melt (H_2O_{melt}, in wt%), percent of crystallisation (wt% melt) and temperature (T, in °C) was fitted to a linear function of the form :

$$\text{wt\% melt} = (a\,T + b)\,H_2O_{melt} + c\,T + d \qquad (2)$$

The regressed parameters *a,b, c* and *d* are listed in Table 2. At pressures up to 400 MPa, for each composition at any given P and T, the relationships between H_2O_{melt} and fH_2O was calculated using the following empirical equation :

$$fH_2O = e\,H_2O_{melt}^{f} \qquad (3)$$

The parameters *e* and *f* of equation 3 were derived at any P and T (Table 3) for each composition so as to produce the H_2O_{melt} obtained at H_2O saturation in the experiments, using fH_2O for pure water at the relevant P and T from Holland and Powell equation of state (Holland & Powell, 1991). For experiments at higher pressures, it was found easier to use different mathematical expressions (see Table 3). Although derived from H_2O-saturated experiments, equation (3) was also used for calculating the melt water content at under-saturated conditions (ie CO_2-bearing). The reason for regressing systematically *e* and *f* values specific to any composition at P and T is to facilitate the finding of the numerical solution during the iteration procedure seeking for the conditions of equilibrium distribution of H_2O

and CO_2 between melt and fluid. Use of a single general equation may yield spurious values of melt fraction (ie slightly negative values) that prevent from finding the exact solution. This was avoided by ensuring that the melt fraction at H_2O saturation is exactly consistent with the melt solubility defined by the experiments.

To relate dissolved CO_2 to fCO_2, the same functional relationships than for water was used. In contrast to water, however, many phase equilibrium studies do not report dissolved CO_2 content of quenched melts, hence this parameter has to be estimated. For silicic to intermediate liquids, owing to their much lower solubility of CO_2 relative to H_2O, and the small compositional dependence of CO_2 solubility of such melts, only one set of *e* and *f* values (e=8.23 10^{-6}, f=0.5145) was adopted: *e* and *f* were fitted so as to give a solubility of 0.5 wt% CO_2 at 10 kbar for a pure CO_2 fluid, in agreement with high pressure solubility data on silicic melts (Stolper et al., 1987 ; King & Holloway, 2002 ; Tamic et al., 2001 ; Behrens et al., 2005). For basalts the relationships derived by Lesne et al (2010a,b) for the Stromboli basalt were used. There are some uncertainties as to whether incorporation of H_2O enhances significantly CO_2 solubilities at high pressures. However, calculations performed in which the equation was tuned so as to give twice the solubility value of CO_2 showed only a trivial effect on the final calculated melt fraction.

Knowing the H_2O and CO_2 initially dissolved in the magma, the amount of fluid added to it, as well as its composition (XH_2O_{fluid}), the total amount of H_2O and CO_2 present in the system can be calculated (H_2O_{tot} and CO_{2tot}).

The fluid phase is assumed to be a binary mixture of H_2O and CO_2. The fugacities of H_2O and CO_2 in the fluid (fH_2O_{fluid}, fCO_{2fluid}) are calculated using fugacity coefficients of pure H_2O and CO_2 ($\gamma H_2O°$, $\gamma CO_2°$), calculated at P and T from the equation of state of Holland & Powell (1991), from the following standard thermodynamic relationships :

$$fH_2O_{fluid} = XH_2O_{fluid}\ \gamma H_2O°\ P \qquad (4)$$

$$fCO_{2fluid} = XCO_{2fluid}\ \gamma CO_2^{\circ}\ P \qquad (5)$$

together with the constraint :

$$XH_2O_{fluid} + XCO_{2fluid} = 1 \qquad (6)$$

Arc magmas contain sulfur bearing species (H_2S and SO_2) as well as halogens. The mole fraction of sulfur species in magma reservoirs is in general lower than 0.05 (Scaillet & Pichavant, 2003; Lesne et al., 2015); that of halogens is even lower, and for the sake of simplicity they have been neglected in this work. Incorporation of these species will lower the calculated XH_2O_{fluid} by a small extent (less than 0.05). The addition of fluid is assumed to take place at constant redox state, which is unlikely to be true in real systems. However, there are only limited quantitative experimental data on fO_2 variations in magmas, which do not allow to properly evaluate the effect of changing fO_2 on melt fraction trends, and even less to model them quantitatively in an approach such as the present one. In Fe-poor silicic magmas they can be anticipated to be of second order importance, if fO_2 affects mostly the stabilities of Fe-bearing minerals (but see Scaillet et al., 1997). The experimental work of Martel et al. (1999) explored the effect of varying fO_2 on phase relations and proportions of andesite magmas. They show that modest changes in fO_2 may produce significant variations in melt proportions. For instance, a series of runs performed at around 2.2 kb and 930°C and H_2O saturation but different fO_2 (runs X10, X9 and X6) show the following melt proportions : 87 wt% at NNO+2.2, 77 wt% at NNO+1.2 and 72 wt% at NNO+0.9 (fO_2 being referenced to the NNO solid buffer). This suggests that if fluid infiltration goes along with fO_2 change, it may also contribute to alter significantly the melt fraction.

For a given composition, and P, T, bulk volatile conditions, the program seeks iteratively the melt fraction and temperature set of values which fullfills the following criteria:

$$fH_2O_{melt} = fH_2O_{fluid} \qquad (7)$$

$$fCO_{2\ melt} = fCO_{2\ fluid} \qquad (8)$$

$$H_2O_{tot} = H_2O_{melt}+H_2O_{fluid} \quad (9)$$

$$CO_{2tot}=CO_{2melt}+CO_{2fluid} \quad (10)$$

in addition to the condition of energy conservation. Values adopted in this work for the heat capacities of liquid, solid and gas, and for the latent heat of solids are given in Table 4. Iterations are stopped when species fugacities between two iterations differ by less than 0.1 bar and heat balance differs by less than 0.1 joule.

RESULTS

The details of numerical calculations to evaluate the effect of fluid infiltration on the melt fraction of rhyolite, dacite, andesite and basalt compositions at various pressures using relevant phase equilibrium constraints are provided below.

Rhyolite

Calculations for silicic magmas are first shown for the minimum melt composition in the ternary hapogranite system at 200 MPa (Fig. 3a,b). The starting conditions are 700°C and a melt H_2O content of 4 wt% (XH_2O_{fluid}=0.6), which give a crystal content of ca 30 wt%. These are conditions broadly similar to those inferred for some rhyolites ejected during caldera forming eruptions (e.g. Hildreth, 1981; Wallace et al., 1995). The effect of flushing of such a magma by fluids having XH_2O_{fluid} ranging from 0.9 down to 0.05, is shown on Fig. 3a, whilst the corresponding temperature changes are given on Fig. 3b. For these starting conditions, it can be seen that fluids with XH_2O_{fluid} lower than ca 0.6 produce an increase in magma crystallinity, whilst the reverse is observed for XH_2O_{fluid} >0.6. In contrast, infiltration of such a magma by fluids having an XH_2O_{fluid} =0.6 will not change crystallinity. The more different from this equilibrium XH_2O_{fluid} value is the composition of the infiltrating fluid, the more important is the change in crystallinity. Changes are not symmetrical, however, ie they are more pronounced for fluids with XH_2O_{fluid} <0.6. Crystallinity changes are also not linearly

correlated with amount of fluid added, being more important during the first increments of fluid addition (ie up to 10-15wt%), after which trends tend to flatten toward near equilibrium values, except for the driest fluids (XH_2O_{fluid} <0.3). The calculated temperature changes remain in all cases relatively modest, being less than 20°C for the driest case explored (Fig. 3a). They are positive when the magma crystallises, and negative in the converse case.

The same calculations are shown for a natural rhyolitic composition (Klimm et al., 2003), which differs from the previous case by having Fe, Ca, Ti and Mg elements, which impart different melt fraction trend (Fig. 3c). In the case shown, the starting magma is at 700°C with 6 wt% dissolved H_2O, corresponding to a crystal load of about 20 wt%. In that case the equilibrium fluid composition has an XH_2O_{fluid} = 0.95, reflecting the near water saturated condition (at 200 MPa). As a result, fluid infiltration invariably results in crystallisation of the pervaded magma, the extreme case explored (XH_2O_{fluid} =0.4) even reaching solidus conditions after addition of 15 wt% fluid. It is worth noting that the addition of 1 wt% fluid to such a felsic reservoir leads already to a dramatic increase of its crystallinity, from about 20 wt% to over 40 wt% for an incoming fluid having XH_2O_{fluid} =0.4 (corresponding to a shift of the equilibrium XH_2O_{fluid} from 0.95 down to 0.83): as stated above, the mass of mafic magma needed to supply such an amount of fluid would be broadly similar to that of the resident magma. The corresponding temperature changes are more significant than for the haplogranite, reaching +60°C for the case XH_2O_{fluid} =0.4. As in the previous case, it can be seen that most of the changes occur during the first 10 wt% of fluid addition. The differences between the haplogranite and natural rhyolite are related to the differences in melt fraction trends, the first composition having lower crystallisation temperatures than the latter. The third case correspond to a silicic magma stored at 400 MPa (Scaillet et al., 1995), with 6 wt% dissolved H_2O at 700°C (Fig. 3e,f). The same general patterns of crystal changes are observed, the equilibrium fluid composition having an

XH_2O_{fluid} of 0.55. A difference in temperature change can be noted, however, for the case of melting (XH_2O_{fluid}>0.55) : melting results first in a drop of temperature of ca 15°C, followed by a small increase after 8 wt% of fluid addition : this feature corresponds to the heat added by the H_2O-rich incoming fluid, part of the water being dissolved in the liquid.

Dacite

The case of a dacite composition is shown in Fig. 4a,b, at 200 MPa, 780°C, and H_2O-rich conditions (6-7 wt% H_2O), corresponding to crystal contents of 40-60 wt%, typical for arc dacites (Scaillet & Evans, 1999; Prouteau and Scaillet, 2003) or the so called monotonous crystal-rich intermediate magmas in arc settings (Christiansen, 2000; Bachmann et al. 2002). A melt water content of 7 wt% being close to H_2O saturation at 200 MPa implies that virtually any incoming fluid will end up increasing magma crystal content, most of the increase again occurring over the first 10 wt% of fluid increment. Associated temperature changes remain in all cases small, <15°C, being more marked when crystallisation takes place at low XH_2O_{fluid} (Fig. 4b). For the case of 6 wt% H_2O (60 wt% crystals), an ingress of a near H_2O-pure fluid (XH_2O_{fluid} = 0.95) produces a decrease in crystal content of less than 10 wt% (Fig. 4a). Increasing pressure to near 400 MPa does not alter these crystallisation/melting changes resulting from the incoming of fluids with different compositions relative to that of the equilibrium one (Fig. 4c), except that temperature changes are even smaller (±5°C, Fig. 4d), being slightly negative when the system crystallises.

The case at 960 MPa (Fig. 4e, f) simulates deep crustal storage and processing of magma bodies (Hildreth, 1981, 2020; Hildreth and Moorbath, 1988), as also elaborated on experimental and thermal grounds in models for silicic magma production in arc settings (e.g., Prouteau and Scaillet, 2003; Annen et al., 2006; Cashman et al., 2017). Infiltration of H_2O-rich fluids (XH_2O_{fluid} =0.8, 0.7) into a dacitic mush at 750°C, with 10 wt% dissolved H_2O and 45 wt% crystal, will produce a drastic decrease of its crystal content after 10 wt% fluid

addition (Fig. 4e), associated to a rise in temperature of about 30°C (Fig. 4f). Conversely, as observed at lower pressures, a fluid with an XH_2O_{fluid} =0.5 will led to further crystallisation (Fig. 4e), accompagnied by a drop in temperature (Fig. 4f). It is hence immediately apparent from this example alone that in the deep crust there is more room for remelting partly crystallised magma bodies, as compared to what can occur in upper crust, where most of intermediate to felsic reservoirs have H_2O conditions close to water saturation.

Andesite

For the andesite composition (Fig. 5), the P-T conditions were selected so as to mirror those derived for pre-eruption conditions at Mt Pelée and Montserrat andesitic volcanoes (e.g., Martel et al., 1998 ; Barclay et al. 1998). As for their more silicic counterparts, melt fraction evolution shows significant changes upon the first 1-5 wt% addition of fluid (Fig. 5a,c). Thereafter any increment of fluid produces relatively modest changes, near steady state melt fraction being reached at > 20 wt% fluid. In all cases, temperature changes remain small (Fig. 5b,d), <15°C, being more marked at 400 MPa (Fig. 5d). As shown for the dacite composition, infiltration of a near H_2O-saturated andesite magma body stored in shallow crust (Fig. 5a, case 6.9 wt% H_2O), as inferred for both Mt Pelée and Montserrat magma reservoirs (e.g., Martel et al., 1998 ; Barclay et al. 1998), is inevitably characterised by an increase in its crystal content. Although the crystal increase remains relatively minor in the cases shown, (10-15 wt%), it is large enough to drive the system beyond the critical rheological threshold separating immobile from mobile magma mushes. For instance, as shown in Fig. 5a, an andesite magma at 850-875°C percolated by 5-10 wt% fluid at XH_2O_{fluid}=0.2-0.5 would see its crystal load to increase from 43 wt% to near 60 wt%, ie higher than the mobility threshold of crystal-rich mushes, which is thought to occur at around 50 wt% crystallisation (Vigneresse et al., 1996).

At Montserrat, petrological and experimental studies have come to the conclusion that basalt input at the base of the shallow reservoir lead to partial rejuvenation of the andesite body (Couch et al., 2001; Devine et al., 2003), marked by a 30-50°C temperature increase, with little to no mass transfer from underplated basalt, other than volatiles. Remelting has been attributed to convective self mixing (Couch et al., 2001) but could be due to advective heat transport via bubbles (Bachmann and Bergantz, 2005). The results shown above show that the latter mechanism is probably not powerful enough to explain the documented T increase (unless the temperature of the incoming gas is much hotter than the resident magma, as discussed above). On the other hand, volcanic gas data suggest that a significant part of gases vented from this active dome, but others as well, must come from basalt degassing (e.g., Young et al., 1998; Bani et al., 2022). This suggests that fluid supply from degassing basalt reached steady state across the andesite magma column, or at least that a significant part of the basaltic fluid supplied had time to percolate through the andesite mush so as to reach the open atmosphere. The fact that evidence of remelting is documented rather than crystallisation suggests that in this specific case advective heat transfer has been much more efficient than chemical exchange between bubbles and melt on this time scale of observation.

On Fig. 6 are shown the crystallisation/melting and temperature trends obtained from the high pressure phase equilibria of a mafic andesite (Alonso Perez et al., 2009). The calculations consider the case of an andesite with 10 wt% dissolved H_2O intruded at either 800 or 1200 MPa. It is indeed conceivable that high pressure fractionation of an H_2O-rich arc basalt may produce such H_2O-rich derivatives (e.g., Sisson and Grove, 1993; Pichavant et al., 2002a). Compared to previous examples, the most remarkable feature is that, except for very H_2O-poor fluids (XH_2O_{fluid} <0.2), fluid infiltration is accompagnied by significant re-melting of the original andesite magma body (Fig. 6a,c). For instance, the dacite case shows that a fluid with XH_2O_{fluid}=0.5 arriving into a dacite magma with 12 wt% H_2O_{melt} at about 10 kb,

leads to its crystallization (Fig. 4e). The decrease in crystal content is accompagnied by a considerable temperature increase, up to 70-90°C in the case of andesite stored at 800 MPa and fluxed by a fluid with an XH_2O_{fluid} =0.9 (Fig. 6b). As pointed out previously, this temperature increase is the consequence of the addition of H_2O-rich fluids whose heat capacity is 2-3 times higher than those CO_2-rich, and as a consequence they bring more heat to the system. As a test of this phenomenon, a simulation with a heat capacity of H_2O tuned to a value identical to that of CO_2 produced a temperature increase of 15°C for the case of andesite at 900°C and 800 MPa fluxed by a fluid with XH_2O_{fluid} =0.9 (as opposed to 90°C).

Basalt

Although basalt is ultimately the source of fluids percolating through felsic to intermediate magma bodies, there is growing evidence that fluid flushing of basalt plumbing systems is also common (e.g., Spillaert et al., 2006 ; Aiuppa et al., 2007; Allard, 2009). The calculations done for basalt compositions (Berndt et al., 2005 ; Di Carlo et al., 2006 ; Freise et al. ; 2009) are displayed in Fig. 7. At 200 MPa, a basalt at 1140°C with 2-3 wt% H_2O, which are close to near liquidus conditions inferred for some primitive arc basalts (e.g., Di Carlo et al., 2006; Pichavant et al., 2002), will require incoming fluids particularly dry (XH_2O_{fluid} <0.2) in order to crystallise further (Fig. 7a). Lowering temperature to 1050°C at the same H_2O content increases the starting crystal load to over 70 wt% (Fig. 7a), and any fluid wetter than XH_2O_{fluid} =0.2 will induce melting, the extent of which remains limited however, <20 wt% (Fig. 7a). The temperature change associated to this process remains very small, except for the case of crystal-rich conditions, where it decreases by ca 25°C (Fig. 7b). Increasing pressure to 500 MPa (Fig. 7c,d), does not alter significantly those patterns, changes in temperature being virtually non existent. The case of Stromboli is also shown (Fig 7e,f) since this volcano is the archetype of CO_2-flushing through the plumbing system of basaltic arc volcanoes (e.g., Allard, 2009). A reservoir at 400 MPa, holding a basalt magma at 1140°C

with 3 wt% dissolved H_2O, will remain immune to fluid fluxing at this depth as long as the fluid has a composition of XH_2O_{fluid} =0.2 (Fig. 7e). Conversely, if the same reservoir contains a basalt magma at 1050°C, 2 wt% dissolved H_2O, its infiltration by fluids with XH_2O_{fluid} >0.2 will induce its re-melting (Fig. 7e). As noted above, in all cases, associated temperature changes do not exceed 15°C. This last feature is a consequence of the high latent heat value of mafic magmas (Table 3), whose re-melting thus requires more energy input relative to the case of silicic magma bodies.

DISCUSSION

The above calculations show that variations in the composition of fluids entering stagnant magma bodies may give rise to contrasted patterns of melt fraction evolution, even under near isothermal conditions. Magmas at low temperatures are more sensitive to fluid infiltration than those hotter, because the range in melt H_2O content between H_2O-saturation and solidus increases with temperature (Fig. 1) and thus for a given melt H_2O content the melt fraction increases with T. As a result, a magma has a larger buffering capacity against the external infiltration of fluids at higher T relative to lower T. The calculations demonstrate also that relatively minor amounts of fluid (i.e. less than 5 wt%, see for instance the steep curves in Fig. 3c in the range of 1-5 wt% of fluid added) may lead to dramatic changes in crystallinity, and thus magma rheology, provided that the incoming fluid composition is different from that of the host magma. Thus, the possibility for a magma body to have its crystal load radically altered by chemical exchange with the added fluid is a factor that needs to be considered when modelling the fluid dynamics of magma bodies (e.g., Carrichi et al., 2018). The ultimate effect depends obviously on the amount of mafic magma underplating the silicic layer at any one time, as well as on the volatile endowment of the former: as a rule of thumb, a mafic magma batch carrying 2 wt% volatiles, of which half is CO_2 (i.e. 1 wt%, as inferred for

primary arc magmas (e.g., Plank and Manning, 2019)), will need to be half the size of the silicic reservoir if this one is to be fluxed by 1 wt% mafic fluid (dominated by CO_2 owing to its low solubility in silicate melts in upper crust). The rate of volcanic output of basalt magmas ranges widely from 10^{-5} to 1 km^3/year, but average values are in the 10^{-2} to 10^{-3} km^3/year range in most tectonic settings (White et al., 2006), except for hot spot which ranges from 10^{-2} to 10^{-1} km^3/year. These rates imply that a 1 km^3 silicic body could be underplated by an equivalent volume of basalt in about 100-1000 year in arcs, or 10-100 years in hot-spots. Considering an extrusive to intrusive ratio of 1/5 (White et al., 2006), these time intervals could be reduced by up to a factor of 5. In all likelihood, small silicic reservoirs will be more affected than larger ones by telescoping dykes if both reservoirs are fed at the same rate (i.e. at the same frequency of upward propagating magma batches delivering the same amount of magma), but transient crises with enhanced mafic recharge at large silicic centers may also occur (e.g., Druitt et al., 2012) and release potentially large amounts of CO_2 on shorter time scales. In any case, whether this fluid permeates the main body or escapes sideway will be also a controlling factor.

Temperature changes associated to fluxing have been computed here using standard values for thermodynamic parameters (Cp, latent heat), and range from significative (>50°C) to less than 20°C: in the latter case, the temperature change would be barely detectable even by the best calibrated thermometer (ie the FeTi oxides geothermometer, (Ghiorso and Evans, 2008)). It is worth stressing out that those parameters are not well constrained for hydrous silicate magmas, owing to the technical difficulties in retrieving thermodynamic constants at the elevated pressures and temperatures required to hold volatiles in solution into silicate melts (e.g. Clemens and Navrotsky, 1987), and the above results might need to be reconsidered in light of future development in this field. A further potential limitation is that the effect related to the heat of water exsolution has been neglected, a valid assumption at low

pressure and for silicic melts (exsolution decreases slightly T), but not necessarily at high pressures and for mafic melts (Richet et al., 2000). The calculated T changes are however similar in magnitude to those retrieved by Carrichi et al. (2018) using the MELTs thermodynamic model. Asides from this aspect, the calculations illustrate that the direction of change, that is whether a decrease or an increase in T occurs, strongly depends on the prevailing conditions, including magma composition, prior to fluid infiltration. Perhaps most interesting is the fact that crystallisation may occur at increasing temperature (for instance Fig. 3 E,F), while re-melting can be accompagnied by a decrease in temperature, both trends being opposite to what common sense generally predicts. This is the case in particular of silicic magmas stored at pressures higher than 200 MPa (Fig. 3). The same trend is observed for a crystal-rich basalt magmas, which remelts upon ingress of an XH_2O_{fluid} =0.8, producing a decrease of 30°C (Fig. 7A,B). This is due to the latent heat either consumed or released by the magma during fluid ingression and equilibration. From the petrological standpoint, such a phenomenon will give rise to compositional zoning of minerals that may not be easy to interpret (note again here that if the temperature of the incoming fluid is much hotter than the resident magma, the heat brought by the fluid may overcome the crystallization effect arising from CO_2 addition).

Near liquidus basaltic magmas (that is, crystal-poor) are relatively little affected by fluid flushing (with respect to their crystal load), even when extremely dry fluids are percolating (XH_2O_{fluid} <0.1) (Fig 7A, B), and in such a case, the petrological imprint of fluid fluxing may be revealed merely via its record in melt inclusions volatile contents provided that kinetic factors are not at work (Pichavant et al., 2013). This is a significant aspect that warrants to be stressed: basaltic magmas, if not quenched against cold silicic reservoirs, may serve as effective media of bubble percolation and transport, hence of mantle degassing, in particular along crustal sections where hydraulic connection between the deep and shallow

parts of the plumbing system is maintained: Erebus system may be one such an example (Oppenheimer et al., 2011).

The critical role of the pressure of magma emplacement

The main reason for the effect of pressure illustrated above lies in the contrasted solubilities of H_2O and CO_2 species in silicate melts on the one hand, and, on the other hand, on the fact that volatile solubilities are controlled by species fugacities, other intensive parameters exerting a second order control. In other words, for a fixed melt water content and composition, the corresponding water fugacity will be little affected by variations in P and T. The relationship between fugacity (fi) and composition (Xi) in a fluid is given in equation 4:

$$fH_2O = XH_2O_{fluid}\ \gamma H_2O^\circ\ P$$

in which γH_2O° is the fugacity coefficient that describes departure from non–ideal behaviour. For the sake of simplicity but also to a first good approximation, γH_2O° (and of other volatile species) can be considered as dependent on both T and P but little on fluid composition (i.e. I assume that the fluid can be described as an ideal mixture of non-ideal fluid species). For a silicate melt of known dissolved H_2O content, thermodynamic models allows to calculate the corresponding H_2O fugacity fH_2O (e.g., Blank & Holloway, 1994; Dixon et al., 1995; Zhang, 1999). Since at equilibrium H_2O fugacities in melt and gas phases are equal, it follows that equation (2) allows to calculate the XH_2O_{fluid} of fluids coexisting with hydrous silicate melts at various pressures. Figure 8 shows the results of such calculations performed for various fH_2O (i.e. melt H_2O contents) and temperatures so as to encompass the range of melt T-H_2O conditions of arc magmas. The calculated XH_2O_{fluid} strongly decreases with increasing pressure, such that at 9-10 kb, any magma with melt H_2O contents in the range 2-7 wt% must coexist with a gas phase with XH_2O_{fluid} lower than 0.1. As a result, even CO_2-rich fluids (XH_2O_{fluid}<0.1), such as the one released by a deep-seated basalt, may trigger melting in the

deep crust. In contrast, enhanced crystallisation is an inescapable consequence of fluid migration within silicic magmas if stored at 2 kb with 6 wt% dissolved H_2O (or at 1 kb with 4 wt% dissolved H_2O), unless the mafic fluid has little or no CO_2 at all (Fig. 8). A 6 wt% H_2O magma resting at 2 kb will be melted only if the incoming fluid has an XH_2O_{fluid} >0.96 (ie the fluid composition falls on the right side of the 6 wt% H_2O/780°C curve on Fig 8).

There is no direct control on the composition of fluids coexisting with magmas at mid to low crustal depths. Some insight can be gained from the analyses of melt inclusions (MI) which remain the main source of information on volatiles at depth (e.g., Roggensack et al., 1997 ; Métrich et al., 2001; Luhr, 2001; Cervantes & Wallace, 2003; Métrich and Wallace, 2008), in addition to matrix glasses of lavas erupted in oceanic settings (e.g., Dixon et al., 1988, 1997). To calculate XH_2O_{fluid} from melt inclusions (or matrix glass) in basalts, it is also assumed that only H_2O and CO_2 are present. The XH_2O_{fluid} at equilibrium with the melt inclusion data was calculated by rearranging equation (4):

$$XH_2O_{fluid} = fH_2O/\gamma H_2O^\circ \, P$$

using P as tabulated in the original works, and the thermodynamic model of Dixon et al. (1995) of H_2O solubility in basaltic melts. The relationships between H_2O fugacity and concentration in liquid was retrieved from Dixon et al. (1995), using a second order polynomial function :

$$fH_2O = 75.603(wt\%H_2O)^2 + 70.099\ (wt\%H_2O) - 31.647 \quad (R^2 = 0.9999)$$

To be consistent with this work, the fugacity coefficient of pure water was also calculated using a second order polynomial function fitted to the data listed in Dixon et al. (1995) :

$$\gamma H_2O^\circ = 10^{-08}\, P^2 - 2\ 10^{-05}\, P + 0.9987\ (R^2 = 0.9988)$$

Although primitive arc basalts have liquidus temperatures lower than the 1200°C run temperature of Dixon et al. (1995), in agreement with their elevated water content (e.g., Sisson and Grove, 1993; Plank et al., 2013), possibly at around 1150°C (e.g., Métrich et al.,

2001; Pichavant et al., 2002), this difference introduces a negligible error of the calculated XH_2O_{fluid} values. The slightly lower temperatures will increase $\gamma H_2O°$ (ie increase departure from ideal behaviour) which will thus increase slightly the calculated XH_2O_{fluid}.

Restored mafic fluid compositions using melt inclusions or matrix glass in mafic arc magmas display are shown on Fig. 8, distinguishing the three main geodynamic settings of magma production, arc, hot-spot and mid-ocean-ridge/rift contexts. The considered works (see figure 8 caption), although not exhaustive, provide already a comprehensive view on the dissolved H_2O and CO_2 contents of basaltic magmas.

This MI/matrix glass-based data on basalt fluids can be compared to the equilibrium XH_2O_{fluid} of felsic magma reservoirs. For this category, I use data retrieved mostly from phase equilibrium experiments which, though less abundant because time consuming, provide improved constraints on pre-eruptive conditions (see Scaillet and Pichavant, 2003; Scaillet et al., 2016). In the vast majority of cases, corresponding MI also yield similar fluid compositions (XH_2O_{fluid}> 0.8 e.g., Wallace et al., 1999), though the occurrence of MI trapped syn-eruptively will drive some data further toward the XH_2O-rich part of the diagram.

The use of MI assumes that they faithfully mirror the magma volatile contents, which is known not to be the case however (see Barth and Plank, 2021; Wallace et al., 2021, Rose Koga et al., 2021). Melt inclusions can be affected by several post-entrapment processes, in particular loss of H-bearing species during decompression (e.g., Gaetani et al., 2012) or exsolution of CO_2 in a separate bubble (e.g., Hanyu et al., 2020). While the first process will tend to decrease calculated XH_2O_{fluid}, the second will increase it (if not corrected for): though it is difficult to evaluate their respective role, which will vary depending on local conditions, it is likely that CO_2 exsolution skews the MI data base toward H_2O-rich conditions in many instances. In the following, the published values of H_2O and CO_2 contents are nevertheless used at face value, keeping in mind that they may be altered to some extent (in particular by

the occurrence of CO_2-rich bubbles), depending on the conditions specific to the case studied. Yet, the patterns shown below are sufficiently robust that corrections for the above factors are unlikely to change the general conclusions derived from the present analysis.

The XH_2O_{fluid} of arc basalts essentially covers, in an evenly way, all XH_2O_{fluid}-P domain up to 4 kbar (Fig. 8). The highest pressures recorded correspond to dry fluids with $XH_2O_{fluid}<0.1$. The scarcity of high pressure fluids is remarkable, reflecting either the lack of crystallization at high pressure or the re-equilibration of high pressure MI once arriving in shallow magma reservoirs. The extreme variability in fluid composition of arc basalts likely mirrors a similar extreme variation of their sources in terms of their water content (e.g., Cooper et al., 2020). This in turn reflects also the variable conditions reigning in arc settings for magma production, which depends, inter alia, on the lithology being subducted (fresh or altered oceanic crust, serpentinites, contribution of sediments etc…) (e.g., Walowski et al., 2015) and on the geophysical conditions governing subduction (angle and velocity of subduction, age of subducted crust, thickness of mantle wedge…) (e.g. Syracuse et al. 2010). Regardless, the main point is that the vast majority of basalt fluids tends to be significantly H_2O-poor relative to the fluid compositions prevailing in felsic reservoirs in arc settings as inferred from phase equilibria (e.g., Scaillet and Pichavant, 2003). The XH_2O_{fluid} of the latter readily cluster in the H_2O-rich part of the diagram, showing that basalt underplating at pressures below 4 kb will lead to crystallization of the magma body on a long term basis. Note that this trend will be further exacerbated if CO_2 exsolution into separate bubbles would be accounted for in the data base, since bubble occurrence accommodates a significant part of the CO_2 budget of MI (40 to 90%, Moore et al., 2015).

The two other geodynamic contexts display radically different patterns, plotting in the left part of the diagram, showing that corresponding basalts coexist with CO_2-rich fluids until near surface conditions, as amply demonstrated by previous work (e.g., Moore, 1970, 1979;

Dixon et al., 1988; Bottinga and Javoy, 1989; Javoy and Pineau, 1991; Pineau and Javoy, 1994; Dixon et al., 1997; Bureau et al., 1998; Saal et al., 2002; Aubaud et al., 2004, 2005; Chavrit et al., 2014; Hauri et al., 2018; Jones et al., 2020). Ridge-related basalts define the driest and smallest field in such a projection, while hot-spot basalts produce fluids that extend towards higher XH_2O_{fluid} at low pressure, reflecting their higher water content compared to MORBs (e.g., Hudgins et al., 2015), hence occupying an intermediate position between arc and ridge magmas. As with arc magmas, these two patterns reflect source conditions, i.e. a dry depleted mantle for ridge basalts (e.g., Saal et al., 2002) and a somewhat wetter (and deeper) and enriched mantle for hot-spot magmas (e.g., Dixon et al., 1997). The fact that hot spot magmas trend toward H_2O-richer fluids at low pressure reflects in part the shallower pressures recorded by matrix glasses of pillow lavas relative to those of MI (see for instance Dixon et al., 1991; Oppenheimer et al., 2018). Interestingly, from the viewpoint of H_2O-CO_2 composition, both ridges and hot-spot basalts extend toward a common "point" at high pressure, in stark contrast with the widely dispersed pattern shown by arc basalts. This is obviously the consequence of the elevated solubility of water in silicate melts relative to CO_2, and of the relative limited variability of the H_2O content in ridge and hot-spot (ie 0.1-1 wt% H_2O) compared to arc (>1 to over 10 wt% H_2O) basalts: at high pressure essentially all H_2O is strongly partitioned into the liquid. As a result, the significant variability inferred for the sub-oceanic mantle CO_2 content worldwide (e.g. Le Voyer et al., 2019) does not reflect in the fluid composition at high pressure. Available experimental or analytical constraints on the pre-eruptive conditions of felsic reservoirs in such settings indicate that, apart from a few cases (ex Erebus phonolite with an H_2O_{melt} of 0.1 wt%, corresponding to a XH_2O_{fluid}<0.1 at 0.2-1 kbar, Moussallam et al., (2013)), felsic magmas in such environments are quite H_2O-rich (e.g., Webster et al., 1993; Wilding et al., 1993; Scaillet and Macdonald, 2001; 2006; Harms et al., 2004; Freise et al., 2003; Andujar et al. 2010, Andujar and Scaillet, 2013; Di

Carlo et al., 2010; Lucic et al., 2016; Romano et al., 2018; Iddon and Edmonds, 2020), with pre-eruptive H_2O content of 3-5 wt%, very little if any CO_2 (hence XH_2O_{fluid} =1), at pressures of 1-3 kb, ie occupying a position similar to those of arc-magmas. This reflects the overall incompatible behaviour of H_2O in crystallising magmas, and the extreme degree of fractionation of parental magmas that felsic daugthers produced in ridges or hot-spot contexts require (e.g., Macdonald et al., 2021). Anyway, the very CO_2-rich nature of high pressure fluids in ridges and hot spot settings indicates that underplating of magmas in the crust of such settings will likely favour crystallization rather than melting. A significant outlier to this rule is represented by the Erebus system (rift context), whose phonolite lava lake (hence filled by nearly dry melt) is fluxed permanently by CO_2-rich gases (e.g., Oppenheimer et al., 2011): in that case, the heat brought up by basaltic fluids seems capable of maintaining the magma column significantly melted up to the surface, overcoming the dessicating effect of CO_2 percolation. A possible facilitating factor may be the relatively low viscosity of phonolitic liquids relative to rhyolites in arc settings (Andujar and Scaillet, 2012), which allows faster CO_2 transfer (ie fast enough to prevent full chemical equilibrium, but slow enough to allow heat transfer and bubble uptake of fast diffusing species such as H_2O).

For arc systems, the partial overlap of XH_2O_{fluid} between silicic and basalt fluids shows that in some cases mafic fluids may remelt felsic magma bodies stored in upper crust, which will thus amplify any thermal effect associated to heat advection by bubbles (Bachmann & Bergantz, 2005). In general, however, the data suggest that fluid supply from mafic arc magmas in the upper crust will crystallise, rather than melt, shallow felsic magmas (unless the fluid injected is much hotter than the resident magma). Thus, although basalt intrusion at the base of shallow silicic reservoirs can impart transient remelting with fluid dynamic instabilities driving the system toward eruption (e.g., Couch et al., 2001), on a long term basis, the dominant effect of mafic fluid supply to magma bodies in the shallow crust is

one of crystallisation. Complete crystallisation under near isothermal conditions is even conceivable, provided that the fluid has a composition akin to reach the solidus of the plutonic body (case D, Fig. 2,). In this respect, solidification of magmas may occur at a different rate than by heat dissipation alone, be it via conduction or convection, basically at a rate controlled by bubble flux (as long as bubbles can move across the mush). Thus, bubble migration is likely to exert a significant control on the longevity of shallow crustal reservoirs, that could partially offset the thermal effects associated to heat input from basalt. At the other end of the pressure range, fluid supply to plutonic bodies in the deep crust may trigger, or maintain, partially molten conditions, which should enhance the potential for silicic magma production and differentiation at depth. This finding is in line with recent thermal modelling results that have shown that the deep crust is a more favorable locus for silicic melt generation and storage over protracted periods than is the shallow crust (e.g., Dufek and Bergantz, 2005; Annen et al., 2006 ; Solano et al., 2012). Prolonged partial melting of the deep crust to sustain batholith growth in arc settings is required not only by thermal arguments, but also by chemical considerations. Below I address the questions of how rich is the lower crust in fluid and what could be the composition of fluids entering the lower crust in arc settings.

Amount, composition and flux of fluid in the deep crust

In arc settings, the amount of fluid potentially available at the base of the crust, as well as its composition, have been variably assessed combining He fluxes and isotopes, melt inclusion and volcanic gas constraints (e.g., Fischer & Marty, 2005; Wallace, 2005; Plank and Manning, 2019). Such studies have concluded that primitive melts in the mantle wedge have CO_2 contents close to, or in excess of, 1 wt%. The amount of H_2O carried by mantle melts in the sub arc is more difficult to constrain but estimates range up to 16 wt%, for 20 % partial melting of the mantle source assuming a molar H_2O/CO_2 ratio of 25 (e.g., Fischer & Marty,

2005). Based on melt inclusion systematics, Wallace (2005) estimated that a H_2O/CO_2 ratio of 4 is more reasonable. Regardless the exact initial H_2O/CO_2 ratio, the retrieved volatile contents of arc magmas in the mantle are generally high enough to promote fluid saturation of silicate melts at the base of a normal arc crust (ie 30 km thick), in particular if some fractionation is to occur there to shift from melts at equilibrium with mantle residue (high MgO basalts) toward more common high alumina basalts (e.g. Pichavant et al., 2002b) which are likely to feed upper crustal reservoirs. For instance, the calculated XH_2O_{fluid} at 10 kbar of an hypothetical mantle magma (basalt) having a bulk volatile content of 16 wt% with a mole H_2O/CO_2 ratio of 4, using the approach outlined above, is 0.79. According to Fig. 8, such a XH_2O_{fluid} value implies that, depending on the local geotherm, the first fluids released by arc basalts ponding at the base of the crust may trigger crustal melting. Modelling has shown that temperatures of around 800°C prevail at the base of a 30 km thick arc crust beneath the volcanic front (e.g., Furukawa, 1993). This is well above the H_2O-saturated solidus of silicic or basaltic composition at this depth (<700°C, Schmidt & Poli, 1998; Ebadi and Johannes, 1991), but below that defined by CO_2-rich fluids (see below). Considering that the XH_2O_{fluid} of the bulk volatile carried by mantle melts in arcs is at least of 0.79 (for a H_2O/CO_2 ratio of 4, or 0.96 for a H_2O/CO_2 ratio of 25), complete solidification of mantle magmas at the base of the crust should release fluids whose compositions are more than likely able to initiate crustal melting even without the associated heat input (see Figures 4,7). In the two other settings, high pressure fluids have $XH_2O<1$ (Fig. 8). The solidus of granite at 10 kb for an XH_2O_{fluid} of 0.1, is around 900°C, or 1000°C for XH_2O_{fluid}=0.05 (Ebadi and Johannes, 1991), ie significantly higher than dehydration melting temperatures of amphibole-or micas-bearing lithologies (750-850°C) (e.g., Rapp and Watson, 1995; Patino Douce and Harris, 1998). Thus, the melting of the lower crust under such conditions (fluid present and CO_2-rich) requires higher temperatures, hence high fluxes of basalt injection (e.g., Dufek and Bergantz, 2005;

Annen et al., 2006). Overall, it appears that the very CO_2-rich nature of ridges and hot-spot deep fluids (Fig. 8) makes the conditions reigning in the lower crust of such settings much less favourable to melting than in arcs. As a final note, it is worth stressing that the simulations presented above assume that crustal melting occurs under fluid present conditions, while evidence has been put forward for fluid-absent crustal melting in the lower crust (e.g., Clemens and Vielzeuf, 1987; Vielzeuf and Montel, 1994; Clemens and Watkins, 2001; Vielzeuf and Schmidt, 2001). It is worth recalling also that thermal modelling has also generally assumed fluid-absent reactions to model the partial melting of lower crustal lithologies (e.g., Dufek and Bergantz, 2005; Annen et al., 2006), which requires higher temperatures than H_2O-present conditions but lower than those with CO_2-rich fluids. If fluid-present conditions in the lower crust readily represent the common situation attending crustal melting, as the MI and petrological evidence seems to demand, notably in arc settings, this requires a revision of current models of crustal growth based on fluid-absent melting reactions.

Consequences for crust thickness in arcs

Crust thickness in arc settings is well known to correlate tightly with erupted magma major or trace element chemistry, basalts with tholeiitic affinity (high FeO/MgO ratio) occurring in thin arc crust, while those with a calc-alkaline signature (low FeO/MgO ratio) occur in thick arcs (e.g., Myashiro, 1974; Coulon and Thorpe, 1981; Plank and Langmuir, 1988; Turner and Langmuir, 2015; Farner and Lee, 2017; Lieu and Stern, 2019). Crust thickness has also been proposed as a factor controlling ore-processes related to magmatism (e.g., Chiaradia, 2014; Rezeau and Jagoutz, 2020; Lee and Tang, 2020), stressing the importance of understanding processes driving crustal growth. It is noteworthy that above 7-10 kb, essentially any fluid composition, except those really dry as in hot-spot or ridges

settings, will lead to remelting of deep seated felsic or intermediate magma bodies (i.e. fluids released by subduction processes will plot to the right of the 3 solid curves). Such a threshold between fluid imparted crystallisation and fluid triggered melting regimes (7-10 kbar, Fig. 8) corresponds to a pressure depth of about 25-30 km. Such a depth is similar to the average thickness of crust in arc settings, which is 28±11 km regardless of the subduction duration (Gill, 1980). Asides from tectonic processes (e.g., Haschke and Gunther, 2003), the process of crustal growth ultimately demands magma solidification at depth, and it will proceed as long as mafic inputs favour crystallisation instead of melting. This may be the case when the tempo of intrusion is sufficiently slow so as to allow the local geotherm to relax to background value between different intrusive events so that the bottom section of the crust remains below solidus (e.g., Bergantz, 1989; Annen et al., 2006) allowing the crust to grow thicker if not delaminated. In contrast, when the advection of heat is fast, it will raise the ambient geotherm to temperatures above the wet solidus, and the above analysis shows that fluid released by underplated basalts will trigger partial melting. The lower crust, if recurrently partially melted, remains easily remobilisable which allows, or facilitates, material transfer either upward owing to buoyancy or downward by dragging due the convecting mantle wedge or via density-driven foundering of dense rocks (e.g., Jull and Kelemen, 2001; Dufek and Bergantz, 2005; Karlstrom et al., 2014; Zandt et al., 2004; Jagoutz and Behn, 2013; Kelemen and Behn, 2015; Jagoutz and Kelemen, 2015). Hence, one reason for the broadly constant thickness of arc crust worldwide might be the difficulty to crystallise magmas at the base of thick arcs once they reach 25-30 km thickness. One of the limiting factors of crustal growth in arc settings may be, therefore, the extent to which the subducting plate loses its H_2O and CO_2, and how these volatiles are fractionated during transfer through the mantle wedge.

This work has explored essentially the consequences of fluid flushing in terrestrial magmatic systems, owing to the extensive data base available for volatiles in magmas on our

planet. What happens on other planets will depend on their endowment of volatile components (e.g., Greenwood et al., 2018), and the distribution of volatiles among the different envelopes (mantle, crust, atmosphere..) as well as the prevailing geodynamic regime and the various feedback between these parameters. Venus, often presented as the twin planet of Earth, may represent a special case characterized by its dry conditions. Regardless of the mechanisms which made Venus poor in water (initial endowment or late processes) e.g., Kasting and Pollack, 1983; Chassefière, 1997; Kurilov et al., 2006; Chassefière et al., 2012), the possible absence of such a component in Venusian magmas, and lack of plate tectonics, at least for recent times (ie magmatism operates via a hot-spot like process, e.g. Phillips et al. (1991)), may have been factors favouring the grow and stability of a relatively thick crust on this body. In detail, however, considering the errors associated to the estimate of crustal thickness of distant planets (see McLennan, 2022), both Earth and Venus can be said to have approximately the same crustal thicknesses, which contrast with the thicker crusts preserved by smaller bodies, such as Mars, the Moon, or Vesta (McLennan, 2022). These smaller bodies may in fact essentially bear witness of a primordial crust (produced from a magma ocean stage), as opposed to Earth and Venus which are covered by secondary (basalt issued from mantle) or tertiary crust (granite issued from basalt). Hence, since there is currently no way to draw any firm conclusion owing to the scarcity of observations, one can only speculate that the relatively thin crusts of large planets (Earth sized) could reflect *inter alia* the operation of a subduction regime of heat dissipation as we know it today on Earth or which may have been active in more ancient times on Venus.

Acknowledgements. This work is the result of years of laboratory work performed at Orléans. Discussions with Michel Pichavant, Joan Andujar, Stéphane Scaillet, Gaelle Prouteau and Manuel Moreira have helped to clarify many aspects of this paper. Detailed and

insightful reviews by Paul Wallace and an anonymous reviewer helped to refine my arguments and to improve significantly this work. I acknowledge support from both LabEx VOLTAIRE (LABX-100-01) and EquipEx PLANEX (ANR-11-EQPX-0036) projects.

References

Anderson, A. T., & Brown, G. G. (1993). CO_2 contents and formation pressures of some Kilauean melt inclusions. *American Mineralogist, 78*(7-8), 794-803.

Andújar, J., Costa, F., & Martí, J. (2010). Magma storage conditions of the last eruption of Teide volcano (Canary Islands, Spain). *Bulletin of Volcanology, 72*(4), 381-395.

Andújar, J., & Scaillet, B. (2012a). Experimental constraints on parameters controlling the difference in the eruptive dynamics of phonolitic magmas: the case of Tenerife (Canary Islands). *Journal of Petrology, 53*(9), 1777-1806.

Andújar, J., & Scaillet, B. (2012b). Relationships between pre-eruptive conditions and eruptive styles of phonolite–trachyte magmas. *Lithos, 152*, 122-131.

Annen, C., & Burgisser, A. (2021). Modeling water exsolution from a growing and solidifying felsic magma body. *Lithos, 402*, 105799.

Annen, C., & Sparks, R. S. J. (2002). Effects of repetitive emplacement of basaltic intrusions on thermal evolution and melt generation in the crust. *Earth and Planetary Science Letters, 203*(3-4), 937-955.

Annen, C., Blundy, J. & Sparks, R.J.S. The genesis of intermediate and silicic magmas in deep crustal hot zones. *J. Petrol.* **47**, 505-529 (2006).

Alonso-Perez, R., Müntener, O., & Ulmer, P. (2009). Igneous garnet and amphibole fractionation in the roots of island arcs: experimental constraints on andesitic liquids. *Contributions to Mineralogy and Petrology, 157*(4), 541-558.

Aubaud, C., Pineau, F., Jambon, A., & Javoy, M. (2004). Kinetic disequilibrium of C, He, Ar and carbon isotopes during degassing of mid-ocean ridge basalts. *Earth and Planetary Science Letters*, *222*(2), 391-406.

Aubaud, C., Pineau, F., Hékinian, R., & Javoy, M. (2005). Degassing of CO2 and H2O in submarine lavas from the Society hotspot. *Earth and Planetary Science Letters*, *235*(3-4), 511-527.

Bachmann, O. & Bergantz, G.W. Gas percolation in upper-crustal silicic crystal mushes as a mechanism for upward heat advection and rejuvenation opf near solidus magma bodies. J. Volc. Geotherm. Res. 2005.

Bachmann, O., Dungan, M. A., & Lipman, P. W. (2002). The Fish Canyon magma body, San Juan volcanic field, Colorado: rejuvenation and eruption of an upper-crustal batholith. *Journal of Petrology*, *43*(8), 1469-1503.

Bani, P., Oppenheimer, C., Tsanev, V., Sriail'et, B., Primulyana, S., Saing, U. B., ... & Marlia, M. (2022). Modest volcanic SO_2 emissions from the Indonesian archipelago. *Nature communications*, *13*(1), 1-15.

Barclay, J., M. J. Rutherford, & R. S. J. Sparks, Experimental phase equilibria constraints on preeruptive storage conditions of the Soufriere Hills magma, *Geophys. Res. Lett*. **25**, 3437–3440 (1998).

Barth, A., & Plank, T. (2021). The ins and outs of water in olivine-hosted melt inclusions: hygrometer vs. speedometer. *Frontiers in Earth Science*, *9*, 343.

Bergantz, G. W. (1989). Underplating and partial melting: implications for melt generation and extraction. *Science*, *245*(4922), 1093-1095.

Bertagnini, A., Métrich, N., Landi, P., & Rosi, M. (2003). Stromboli volcano (Aeolian Archipelago, Italy): An open window on the deep-feeding system of a steady state basaltic volcano. *Journal of Geophysical Research: Solid Earth*, *108*(B7).

Blundy, J., Cashman, K. V., Rust, A., & Witham, F. (2010). A case for CO2-rich arc magmas. *Earth and Planetary Science Letters*, *290*(3-4), 289-301.

Bottinga, Y., & Javoy, M. (1989). MORB degassing: evolution of CO_2. *Earth and Planetary Science Letters*, *95*(3-4), 215-225.

Brounce, M. N., Kelley, K. A., & Cottrell, E. (2014). Variations in Fe3+/∑ Fe of Mariana Arc basalts and mantle wedge f O2. *Journal of Petrology*, *55*(12), 2513-2536.

Bureau, H., Métrich, N., Pineau, F., & Semet, M. P. (1998a). Magma–conduit interaction at Piton de la Fournaise volcano (Réunion Island): a melt and fluid inclusion study. *Journal of Volcanology and Geothermal Research*, *84*(1-2), 39-60.

Bureau, H., Pineau, F., Métrich, N., Semet, M. P., & Javoy, M. (1998b). A melt and fluid inclusion study of the gas phase at Piton de la Fournaise volcano (Réunion Island). *Chemical geology*, *147*(1-2), 115-130.

Cabral, R. A., Jackson, M. G., Koga, K. T., Rose-Koga, E. F., Hauri, E. H., Whitehouse, M. J., ... & Kelley, K. A. (2014). Volatile cycling of H_2O, CO_2, F, and C l in the HIMU mantle: A new window provided by melt inclusions from oceanic hot spot lavas at Mangaia, Cook Islands. *Geochemistry, Geophysics, Geosystems*, *15*(11), 4445-4467.

Cardoso, S.S. & Woods, A.W. On convection in a volatile-saturated magma. *Earth Planet. Sci. Lett*. **168**, 301-310 (1999).

Caricchi, L., Sheldrake, T. E., & Blundy, J. (2018). Modulation of magmatic processes by CO_2 flushing. *Earth and Planetary Science Letters*, *491*, 160-171.

Cashman, K. V., Sparks, R. S. J., & Blundy, J. D. (2017). Vertically extensive and unstable magmatic systems: a unified view of igneous processes. *Science*, *355*(6331).

Cervantes, P. & Wallace, P.J. Role of H_2O in subduction-zone magmatism : new insights from melt inclusions in high-Mg basalts from central Mexico. *Geology* **31**, 235-238 (2003).

Chavrit, D., Humler, E., & Grasset, O. (2014). Mapping modern CO_2 fluxes and mantle carbon content all along the mid-ocean ridge system. *Earth and Planetary Science Letters*, *387*, 229-239.

Chassefière, E. (1997). Loss of water on the young Venus: The effect of a strong primitive solar wind. *Icarus*, *126*(1), 229-232.

Chassefière, E., Wieler, R., Marty, B., & Leblanc, F. (2012). The evolution of Venus: Present state of knowledge and future exploration. *Planetary and Space Science*, *63*, 15-23.

Chiaradia, M. (2014). Copper enrichment in arc magmas controlled by overriding plate thickness. *Nature Geoscience*, *7*(1), 43-46.

Clemens, J. D., & Navrotsky, A. (1987). Mixing properties of NaAlSi3O8 melt-H2O: New calorimetric data and some geological implications. *The Journal of Geology*, *95*(2), 173-186.

Clemens, J. D., & Vielzeuf, D. (1987). Constraints on melting and magma production in the crust. *Earth and Planetary Science Letters*, *86*(2-4), 287-306.

Clemens, J., & Watkins, J. M. (2001). The fluid regime of high-temperature metamorphism during granitoid magma genesis. *Contributions to Mineralogy and Petrology*, *140*(5), 600-606.

Colman, A., Sinton, J. M., & Wanless, V. D. (2015). Constraints from melt inclusions on depths of magma residence at intermediate magma supply along the Galápagos Spreading Center. *Earth and Planetary Science Letters*, *412*, 122-131.

Couch, S., Sparks, R.J.S. & Carroll, M.R. Mineral disequilibrium in lava explained by convecrive self-mixing in open magma chambers. *Nature* **411**, 1037-1039 (2001).

Coulon, C., & Thorpe, R. (1981). Role of continental crust in petrogenesis of orogenic volcanic associations. *Tectonophysics*, *77*(1-2), 79-93.

Davidson, J., Turner, S., Handley, H., Macpherson, C., & Dosseto, A. (2007). Amphibole "sponge" in arc crust?. *Geology*, *35*(9), 787-790.

Davis, M. G., Garcia, M. O., & Wallace, P. (2003). Volatiles in glasses from Mauna Loa Volcano, Hawai'i: implications for magma degassing and contamination, and growth of Hawaiian volcanoes. *Contributions to Mineralogy and Petrology*, *144*(5), 570-591.

Degruyter, W., Parmigiani, A., Huber, C., & Bachmann, O. (2019). How do volatiles escape their shallow magmatic hearth?. *Philosophical Transactions of the Royal Society A*, *377*(2139), 20180017.

Devine, J.D., Rutherford, M.J., Norton, G.E. & Young, S.R. Magma storage region processes inferred from geochemistry of Fe-Ti oxides in andesitic magma, Soufrière Hills volcano, Montserrat, W.I. *J. Petrol.* **44**, 1375-1400 (2003).

Di Muro, A., Métrich, N., Vergani, D., Rosi, M., Armienti, P., Fougeroux, T., ... & Civetta, L. (2014). The shallow plumbing system of Piton de la Fournaise Volcano (La Reunion Island, Indian Ocean) revealed by the major 2007 caldera-forming eruption. *Journal of Petrology*, *55*(7), 1287-1315.

Dixon, J. E., Stolper, E., & Delaney, J. R. (1988). Infrared spectroscopic measurements of CO_2 and H_2O in Juan de Fuca Ridge basaltic glasses. *Earth and Planetary Science Letters*, *90*(1), 87-104.

Dixon, J. E., Clague, D. A., & Stolper, E. M. (1991). Degassing history of water, sulfur, and carbon in submarine lavas from Kilauea Volcano, Hawaii. *The Journal of Geology*, *99*(3), 371-394.

Dixon, J. E., & Clague, D. A. (2001). Volatiles in basaltic glasses from Loihi Seamount, Hawaii: Evidence for a relatively dry plume component. *Journal of Petrology*, *42*(3), 627-654.

Dixon J. E., Stolper E. M., & Holloway J. R. An experimental study of water and carbon dioxide solubilities in mid-ocean ridge basaltic liquids. Part I: Calibration and solubility models. *J. Petrol.* **36,** 1607–1631 (1995).

Dixon, J.E., Clague, D.A., Wallace, P., Poreda, R. Volatiles in alkalic basalts from the North Arch volcanic field, Hawai : extensive degassing of deep submarine-erupted alkalic series lavas. *J. Petrol*. **36**, 911-939 (1997).

Druitt, T. H., Costa, F., Deloule, E., Dungan, M., & Scaillet, B. (2012). Decadal to monthly timescales of magma transfer and reservoir growth at a caldera volcano. *Nature*, *482*(7383), 77-80.

Dufek, J., & Bergantz, G. W. (2005). Lower crustal magma genesis and preservation: a stochastic framework for the evaluation of basalt–crust interaction. *Journal of Petrology*, *46*(11), 2167-2195.

Ebadi, A., & Johannes, W. (1991). Beginning of melting and composition of first melts in the system Qz-Ab-Or-H_2O-CO_2. *Contributions to Mineralogy and Petrology*, *106*(3), 286-295.

Eichelberger, J.C. Vesiculation of mafic magma during replenishment of silicic magma reservoirs. *Nature* **288**, 446-450 (1980).

Eichelberger, J. C., Chertkoff, D. G., Dreher, S. T., & Nye, C. J. (2000). Magmas in collision: rethinking chemical zonation in silicic magmas. *Geology*, *28*(7), 603-606.

Farner, M. J., & Lee, C. T. A. (2017). Effects of crustal thickness on magmatic differentiation in subduction zone volcanism: A global study. *Earth and Planetary Science Letters*, *470*, 96-107.

Fischer, T.P. & Marty, B. Volatile abundances in the sub-arc mantle : insights from volcanic and hydrothermal gas discharges. *J. Volc. Geotherm. Res.* **140,** 205-216 (2005).

Freise, M., Holtz, F., Koepke, J., Scoates, J., & Leyrit, H. (2003). Experimental constraints on the storage conditions of phonolites from the Kerguelen Archipelago. *Contributions to Mineralogy and Petrology*, *145*(6), 659-672.

Freise, M., Holtz, F., Nowak, M., Scoates, J. S., & Strauss, H. (2009). Differentiation and crystallization conditions of basalts from the Kerguelen large igneous province: an experimental study. *Contributions to Mineralogy and Petrology*, *158*(4), 505-527.

Furukawa, Y. Magmatic processes under arcs and formation of the volcanic front. *J. Geophys. Res.* **98,** 8309-8319.

Gaetani, G. A., O'Leary, J. A., Shimizu, N., Bucholz, C. E., & Newville, M. (2012). Rapid reequilibration of H2O and oxygen fugacity in olivine-hosted melt inclusions. *Geology*, *40*(10), 915-918.

Ghiorso, M. S., & Evans, B. W. (2008). Thermodynamics of rhombohedral oxide solid solutions and a revision of the Fe-Ti two-oxide geothermometer and oxygen-barometer. *American Journal of science*, *308*(9), 957-1039.

Gill, J.B. Orogenic andesites and plate tectonics. Springer Verlag, Berlin, 390 pp (1981).

Greenwood, J. P., Karato, S. I., Vander Kaaden, K. E., Pahlevan, K., & Usui, T. (2018). Water and volatile inventories of Mercury, Venus, the Moon, and Mars. *Space Science Reviews*, *214*(5), 1-32.

Gualda, G. A., Ghiorso, M. S., Lemons, R. V., & Carley, T. L. (2012). Rhyolite-MELTS: a modified calibration of MELTS optimized for silica-rich, fluid-bearing magmatic systems. *Journal of Petrology*, *53*(5), 875-890.

Hanyu, T., Yamamoto, J., Kimoto, K., Shimizu, K., & Ushikubo, T. (2020). Determination of total CO_2 in melt inclusions with shrinkage bubbles. *Chemical Geology*, *557*, 119855.

Harms, E., Gardner, J. E., & Schmincke, H. U. (2004). Phase equilibria of the Lower Laacher See Tephra (East Eifel, Germany): constraints on pre-eruptive storage conditions of a

phonolitic magma reservoir. *Journal of Volcanology and Geothermal Research*, *134*(1-2), 125-138.

Haschke, M., & Gunther, A. (2003). Balancing crustal thickening in arcs by tectonic vs. magmatic means. *Geology*, *31*(11), 933-936.

Hattori, K. High-sulfur magma, a product of fluid discharge from underlying mafic magma : evidence from Mount Pinatubo, Philippines. *Geology* **21**, 1083-1086 (1993).

Hauri, E. (2002). SIMS analysis of volatiles in silicate glasses, 2: isotopes and abundances in Hawaiian melt inclusions. *Chemical Geology*, *183*(1-4), 115-141.

Hauri, E. H., Maclennan, J., McKenzie, D., Gronvold, K., Oskarsson, N., & Shimizu, N. (2018). CO_2 content beneath northern Iceland and the variability of mantle carbon. *Geology*, *46*(1), 55-58.

Head, E. M., Shaw, A. M., Wallace, P. J., Simons, K. W., & Carn, S. A. (2011). Insight into volatile behavior at Nyamuragira volcano (DR Congo, Africa) through olivine-hosted melt inclusions. *Geochemistry, Geophysics, Geosystems*, *12*(10).

Hildreth, W. (1981). Gradients in silicic magma chambers: implications for lithospheric magmatism. *Journal of Geophysical Research: Solid Earth*, *86*(B11), 10153-10192.

Hildreth, W., & Moorbath, S. (1988). Crustal contributions to arc magmatism in the Andes of central Chile. *Contributions to mineralogy and petrology*, *98*(4), 455-489.

Hildreth, W. (2021). Comparative Rhyolite Systems: Inferences from Vent Patterns and Eruptive Episodicities: Eastern California and Laguna del Maule. *Journal of Geophysical Research: Solid Earth*, e2020JB020879.

Holland, T. & Powell, R. A compensated-Redlich-Kwong (CORK) equation for volumes and fugacities of CO_2 and H_2O in the range 1 bar to 50 kbar and 100-1600°C. *Contrib. Mineral. Petrol.* **109,** 265-273 (1991).

Holloway, J.R. & Blank, J.G. Application of experimental results to C-O-H species in natural melts. In Carroll, M.R. & Holloway, J.R (eds), Volatiles in magmas, *Rev. Mineral*. 30, 187-230.

Huber, C., Bachmann, O. & Manga, M. (2010). Two competing effects of volatiles on heat transfer in crystal-rich magmas : thermal insulation vs defrosting. *Journal of Petrology* **51**, 847-867.

Hudgins, T. R., Mukasa, S. B., Simon, A. C., Moore, G., & Barifaijo, E. (2015). Melt inclusion evidence for CO_2-rich melts beneath the western branch of the East African Rift: implications for long-term storage of volatiles in the deep lithospheric mantle. *Contributions to Mineralogy and Petrology*, *169*(5), 40.

Huppert, H.E., Sparks, R.J. & Turner, J.S. Effects of volatiles on mixing in calc-alkaline magma systems. *Nature* **297**, 554-557 (1982).

Iddon, F., & Edmonds, M. (2020). Volatile-rich magmas distributed through the upper crust in the Main Ethiopian Rift. *Geochemistry, Geophysics, Geosystems*, *21*(6), e2019GC008904.

Jackson, M. G., Koga, K. T., Price, A., Konter, J. G., Koppers, A. A., Finlayson, V. A., ... & Kendrick, M. A. (2015a). Deeply dredged submarine HIMU glasses from the Tuvalu Islands, Polynesia: Implications for volatile budgets of recycled oceanic crust. *Geochemistry, Geophysics, Geosystems*, *16*(9), 3210-3234.

Jackson, M. G., Cabral, R. A., Rose-Koga, E. F., Koga, K. T., Price, A., Hauri, E. H., & Michael, P. (2015b). Ultra-depleted melts in olivine-hosted melt inclusions from the Ontong Java Plateau. *Chemical Geology*, *414*, 124-137.

Jagoutz, O., & Kelemen, P. B. (2015). Role of arc processes in the formation of continental crust. *Annual Review of Earth and Planetary Sciences*, *43*, 363-404.

Javoy, M., & Pineau, F. (1991). The volatiles record of a "popping" rock from the Mid-Atlantic Ridge at 14 N: chemical and isotopic composition of gas trapped in the vesicles. *Earth and Planetary Science Letters*, *107*(3-4), 598-611.

Johannes, W., & Holtz, F. (2012). *Petrogenesis and experimental petrology of granitic rocks* (Vol. 22). Springer Science & Business Media.

Johnson, E. R., Wallace, P. J., Cashman, K. V., Granados, H. D., & Kent, A. J. (2008). Magmatic volatile contents and degassing-induced crystallization at Volcán Jorullo, Mexico: Implications for melt evolution and the plumbing systems of monogenetic volcanoes. *Earth and Planetary Science Letters*, *269*(3-4), 478-487.

Johnson, E. R., Wallace, P. J., Delgado Granados, H., Manea, V. C., Kent, A. J., Bindeman, I. N., & Donegan, C. S. (2009). Subduction-related volatile recycling and magma generation beneath Central Mexico: insights from melt inclusions, oxygen isotopes and geodynamic models. *Journal of Petrology*, *50*(9), 1729-1764.

Jones, M. R., Soule, S. A., Liao, Y., Bradsky, H., Le Roux, V., & Klein, F. (2020). Quantitative vesicle analyses and total CO_2 reconstruction in mid-ocean ridge basalts. *Journal of Volcanology and Geothermal Research*, *407*, 107109.

Jull, M., & Kelemen, P. (2001). On the conditions for lower crustal convective instability. *Journal of Geophysical Research: Solid Earth*, *106*(B4), 6423-6446.

Kasting, J. F., & Pollack, J. B. (1983). Loss of water from Venus. I. Hydrodynamic escape of hydrogen. *Icarus*, *53*(3), 479-508.

Kelemen, P. B., & Behn, M. D. (2016). Formation of lower continental crust by relamination of buoyant arc lavas and plutons. *Nature Geoscience*, *9*(3), 197-205.

Kelley, K. A., Plank, T., Newman, S., Stolper, E. M., Grove, T. L., Parman, S., & Hauri, E. H. (2010). Mantle melting as a function of water content beneath the Mariana Arc. *Journal of Petrology*, *51*(8), 1711-1738.

King, P.L. & Holloway, J.R. CO_2 solubility and speciation in intermediate (andesitic) melts : the role of H_2O and composition. *Geochim. Cosmochim. Acta* **66,** 1627-1640 (2002)

Klimm, K., Holtz, F., Johannes, W. & King, P.L. Fractionation of metaluminous A-type granites : an experimental study of the Wangrah suite, Lachlan fold belt, Australia. *Precam. Res*. **124**, 327-341 (2003).

Koleszar, A. M., Saal, A. E., Hauri, E. H., Nagle, A. N., Liang, Y., & Kurz, M. D. (2009). The volatile contents of the Galapagos plume; evidence for H2O and F open system behavior in melt inclusions. *Earth and Planetary Science Letters*, *287*(3-4), 442-452.

Kulikov, Y. N., Lammer, H., Lichtenegger, H. I. M., Terada, N., Ribas, I., Kolb, C., ... & Biernat, H. K. (2006). Atmospheric and water loss from early Venus. *Planetary and Space Science*, *54*(13-14), 1425-1444.

Lee, C. T. A., & Tang, M. (2020). How to make porphyry copper deposits. *Earth and Planetary Science Letters*, *529*, 115868.

Le Voyer, M., Rose-Koga, E. F., Shimizu, N., Grove, T. L., & Schiano, P. (2010). Two contrasting H_2O-rich components in primary melt inclusions from Mount Shasta. *Journal of Petrology*, *51*(7), 1571-1595.

Le Voyer, M., Cottrell, E., Kelley, K. A., Brounce, M., & Hauri, E. H. (2015). The effect of primary versus secondary processes on the volatile content of MORB glasses: An example from the equatorial Mid-Atlantic Ridge (5° N–3° S). *Journal of Geophysical Research: Solid Earth*, *120*(1), 125-144.

Le Voyer, M., Hauri, E. H., Cottrell, E., Kelley, K. A., Salters, V. J., Langmuir, C. H., ... & Füri, E. (2019). Carbon Fluxes and Primary Magma CO_2 Contents Along the Global Mid-Ocean Ridge System. *Geochemistry, Geophysics, Geosystems*, *20*(3), 1387-1424.

Lesne, P., Scaillet, B., & Pichavant, M. (2015). The solubility of sulfur in hydrous basaltic melts. *Chemical Geology*, *418*, 104-116.

Lieu, W. K., & Stern, R. J. (2019). The robustness of Sr/Y and La/Yb as proxies for crust thickness in modern arcs. *Geosphere*, *15*(3), 621-641

Lloyd, A. S., Ruprecht, P., Hauri, E. H., Rose, W., Gonnermann, H. M., & Plank, T. (2014). NanoSIMS results from olivine-hosted melt embayments: Magma ascent rate during explosive basaltic eruptions. *Journal of Volcanology and Geothermal Research*, *283*, 1-18.

Longpré, M. A., Stix, J., Klügel, A., & Shimizu, N. (2017). Mantle to surface degassing of carbon-and sulphur-rich alkaline magma at El Hierro, Canary Islands. *Earth and Planetary Science Letters*, *460*, 268-280.

Lucic, G., Berg, A. S., & Stix, J. (2016). Water-rich and volatile-undersaturated magmas at Hekla volcano, Iceland. *Geochemistry, Geophysics, Geosystems*, *17*(8), 3111-3130.

Luhr, J.F. Glass inclusions and melt volatile contents at Paricutin volcano, Mexico. *Contrib. Mineral. Petrol*. **142**, 261-283 (2001).

Macdonald, R., White, J. C., & Belkin, H. E. (2021). Peralkaline silicic extrusive rocks: magma genesis, evolution, plumbing systems and eruption. *Comptes Rendus. Géoscience*, *353*(S2), 1-53.

Maria, A. H., & Luhr, J. F. (2008). Lamprophyres, basanites, and basalts of the Western Mexican volcanic belt: volatile contents and a vein–wallrock melting relationship. *Journal of Petrology*, *49*(12), 2123-2156.

Marianelli, P., Métrich, N., & Sbrana, A. (1999). Shallow and deep reservoirs involved in magma supply of the 1944 eruption of Vesuvius. *Bulletin of Volcanology*, *61*(1), 48-63.

Marianelli, P., Sbrana, A., Métrich, N., & Cecchetti, A. (2005). The deep feeding system of Vesuvius involved in recent violent strombolian eruptions. *Geophysical Research Letters*, *32*(2).

Martel, C. Pichavant, M., Holtz, F., Scaillet, B., Bourdier, J.L., Traineau, H. Effects of fO_2 and H_2O on andesite phase relations between 2 and 4 kbar. *J. geophys. Res.* **104**, 29453-29470 (1999).

Martel, C., M. Pichavant, J.-L. Bourdier, H. Traineau, F. Holtz, and B. Scaillet, Magma storage conditions and control of eruption regime in silicic volcanoes: Experimental evidence from Mt. Pelée, *Earth Planet. Sci. Lett.* **156**, 89– 99 (1998).

McLennan, S. M. (2022). Composition of planetary crusts and planetary differentiation. In *Planetary volcanism across the solar system* (pp. 287-331). Elsevier.

Métrich, N., Bertagnini, A., Landi, P. & Rosi, M. Crystallisation driven by decompression and water loss at Stromboli volcano (Aeolian islands, Italy). *J. Petrol.* **42**, 1471-1490 (2001).

Métrich, N., Bertagnini, A., & Di Muro, A. (2010). Conditions of magma storage, degassing and ascent at Stromboli: new insights into the volcano plumbing system with inferences on the eruptive dynamics. *Journal of Petrology*, *51*(3), 603-626.

Métrich, N., Allard, P., Aiuppa, A., Bani, P., Bertagnini, A., Shinohara, H., ... & Massare, D. (2011). Magma and volatile supply to post-collapse volcanism and block resurgence in Siwi Caldera (Tanna Island, Vanuatu Arc). *Journal of Petrology*, *52*(6), 1077-1105.

Métrich, N., & Wallace, P. J. (2008). Volatile abundances in basaltic magmas and their degassing paths tracked by melt inclusions. *Reviews in mineralogy and geochemistry*, *69*(1), 363-402.

Métrich, N., Zanon, V., Créon, L., Hildenbrand, A., Moreira, M., & Marques, F. O. (2014). Is the 'Azores hotspot'a wetspot? Insights from the geochemistry of fluid and melt inclusions in olivine of Pico basalts. *Journal of Petrology*, *55*(2), 377-393.

Moretti, R., Arienzo, I., Orsi, G., Civetta, L., & D'Antonio, M. (2013). The deep plumbing system of Ischia: a physico-chemical window on the fluid-saturated and CO2-sustained Neapolitan volcanism (southern Italy). *Journal of Petrology, 54*(5), 951-984.

Moore, J. G. (1970). Water content of basalt erupted on the ocean floor. *Contributions to Mineralogy and Petrology*, *28*(4), 272-279.

Moore, J. G. (1979). Vesicularity and CO_2 in mid-ocean ridge basalt. *Nature, 282*(5736), 250-253.

Moore, L. R., Gazel, E., Tuohy, R., Lloyd, A. S., Esposito, R., Steele-MacInnis, M., Hauri E.H. , Wallace, P.J., Plank, T. & Bodnar, R. J. (2015). Bubbles matter: An assessment of the contribution of vapor bubbles to melt inclusion volatile budgets. *American Mineralogist, 100*(4), 806-823.

Nichols, A. R. L., Wysoczanski, R. J., Tani, K., Tamura, Y., Baker, J. A., & Tatsumi, Y. (2012). Melt inclusions reveal geochemical cross-arc variations and diversity within magma chambers feeding the Higashi-Izu Monogenetic Volcano Field, Izu Peninsula, Japan. *Geochemistry, Geophysics, Geosystems*, *13*(9).

Miyashiro, A. (1974). Volcanic rock series in island arcs and active continental margins. *American journal of science*, *274*(4), 321-355.

Moussallam, Y., Oppenheimer, C., Scaillet, B., & Kyle, P. R. (2013). Experimental phase-equilibrium constraints on the phonolite magmatic system of Erebus Volcano, Antarctica. *Journal of Petrology*, *54*(7), 1285-1307.

Oppenheimer, C., Moretti, R., Kyle, P. R., Eschenbacher, A., Lowenstern, J. B., Hervig, R. L., & Dunbar, N. W. (2011). Mantle to surface degassing of alkalic magmas at Erebus volcano, Antarctica. *Earth and Planetary Science Letters*, *306*(3-4), 261-271.

Oppenheimer, C., Scaillet, B., Woods, A., Sutton, A. J., Elias, T., & Moussallam, Y. (2018). Influence of eruptive style on volcanic gas emission chemistry and temperature. *Nature Geoscience*, *11*(9), 678-681.

Parat, F., Holtz, F., & Feig, S. (2008). Pre-eruptive conditions of the Huerto andesite (Fish canyon system, San Juan volcanic field, Colorado): influence of volatiles (C–O–H–S) on phase equilibria and mineral composition. *Journal of Petrology*, *49*(5), 911-935.

Parmigiani, A., Degruyter, W., Leclaire, S., Huber, C., & Bachmann, O. (2017). The mechanics of shallow magma reservoir outgassing. *Geochemistry, Geophysics, Geosystems*, *18*(8), 2887-2905.

Parmigiani, A., Huber, C., & Bachmann, O. (2014). Mush microphysics and the reactivation of crystal-rich magma reservoirs. *Journal of Geophysical Research: Solid Earth*, *119*(8), 6308-6322.

Parmigiani, A., Faroughi, S., Huber, C., Bachmann, O., & Su, Y. (2016). Bubble accumulation and its role in the evolution of magma reservoirs in the upper crust. *Nature*, *532*(7600), 492-495.

Patiño Douce, A. E., & Harris, N. (1998). Experimental constraints on Himalayan anatexis. *Journal of Petrology*, *39*(4), 689-710.

Phillips, R. J., Grimm, R. E., & Malin, M. C. (1991). Hot-spot evolution and the global tectonics of Venus. *Science*, *252*(5006), 651-658.

Pichavant, M., & Macdonald, R. (2007). Crystallization of primitive basaltic magmas at crustal pressures and genesis of the calc-alkaline igneous suite: experimental evidence from St Vincent, Lesser Antilles arc. *Contributions to Mineralogy and Petrology*, *154*(5), 535-558.

Pichavant, M., Martel, C., Bourdier, J.L. & Scaillet, B. Physical conditions, structure and dynamics of a zoned magma chamber : Mt Pelée (Martinique, Lesser Antilles arc). *J. Geophys. Res*. **107**(B5), 10.1029/2001JB000315 (2002a).

Pichavant, M., Mysen, B. O., & Macdonald, R. (2002b). Source and H_2O content of high-MgO magmas in island arc settings: an experimental study of a primitive calc-alkaline basalt from St. Vincent, Lesser Antilles arc. *Geochimica et Cosmochimica Acta*, *66*(12), 2193-2209.

Pichavant, M., Di Carlo, I., Rotolo, S. G., Scaillet, B., Burgisser, A., Le Gall, N., & Martel, C. (2013). Generation of CO_2-rich melts during basalt magma ascent and degassing. *Contributions to Mineralogy and Petrology*, *166*(2), 545-561.

Pietruszka, A. J., Keyes, M. J., Duncan, J. A., Hauri, E. H., Carlson, R. W., & Garcia, M. O. (2011). Excesses of seawater-derived ^{234}U in volcanic glasses from Loihi Seamount due to crustal contamination. *Earth and Planetary Science Letters*, *304*(1-2), 280-289.

Pineau, F., & Javoy, M. (1994). Strong degassing at ridge crests: The behaviour of dissolved carbon and water in basalt glasses at 14 N, Mid-Atlantic Ridge. *Earth and Planetary Science Letters*, *123*(1-3), 179-198.

Plank, T., & Langmuir, C. H. (1988). An evaluation of the global variations in the major element chemistry of arc basalts. *Earth and Planetary Science Letters*, *90*(4), 349-370.

Plank, T., & Manning, C. E. (2019). Subducting carbon. *Nature*, *574*(7778), 343-352.

Plank, T., Kelley, K. A., Zimmer, M. M., Hauri, E. H., & Wallace, P. J. (2013). Why do mafic arc magmas contain~ 4 wt% water on average?. *Earth and Planetary Science Letters*, *364*, 168-179.

Plechov, P., Blundy, J., Nekrylov, N., Melekhova, E., Shcherbakov, V., & Tikhonova, M. S. (2015). Petrology and volatile content of magmas erupted from Tolbachik Volcano, Kamchatka, 2012–13. *Journal of Volcanology and Geothermal Research*, *307*, 182-199.

Prouteau, G. & Scaillet, B. Experimental constraints on the origin of the 1991 Pinatubo dacite. *J. Petrol.* **44**, 2203-2241 (2003).

Rapp, R. P., & Watson, E. B. (1995). Dehydration melting of metabasalt at 8–32 kbar: implications for continental growth and crust-mantle recycling. *Journal of Petrology*, *36*(4), 891-931.

Rasmussen, D. J., Plank, T. A., Roman, D. C., & Zimmer, M. M. (2022). Magmatic water content controls the pre-eruptive depth of arc magmas. *Science*, *375*(6585), 1169-1172.

Richet, P., Hovis, G., & Whittington, A. (2006). Water and magmas: Thermal effects of exsolution. *Earth and Planetary Science Letters*, *241*(3-4), 972-977.

Robidoux, P., Aiuppa, A., Rotolo, S. G., Rizzo, A. L., Hasni, E. H., & Frezzotti, M. L. (2017). Volatile contents of mafic-to-intermediate magmas at San Cristóbal volcano in Nicaragua. *Lithos*, *272*, 147-163.

Roggensack, K. (2001). Unraveling the 1974 eruption of Fuego volcano (Guatemala) with small crystals and their young melt inclusions. *Geology*, *29*(10), 911-914.

Roggensack, K., Hervig, R.L., McKnight, E.B., Williams, S.N. Explosive basaltic volcanism from Cerro Negro volcano : influence of volatiles on eruptive style. *Science* **277**, 1639-1642 (1997).

Romano, P., Andújar, J., Scaillet, B., Romengo, N., Di Carlo, I., & Rotolo, S. G. (2018). Phase equilibria of Pantelleria trachytes (Italy): constraints on pre-eruptive conditions and on the metaluminous to peralkaline transition in silicic magmas. *Journal of Petrology*, *59*(3), 559-588.

Rose-Koga, E. F., Bouvier, A. S., Gaetani, G. A., Wallace, P. J., Allison, C. M., Andrys, J. A., ... & Zhou, T. (2021). Silicate melt inclusions in the new millennium: A review of recommended practices for preparation, analysis, and data presentation. *Chemical Geology*, 120145.

Ruprecht, P., Bergantz, G. W., & Dufek, J. (2008). Modeling of gas-driven magmatic overturn: Tracking of phenocryst dispersal and gathering during magma mixing. *Geochemistry, Geophysics, Geosystems*, *9*(7).

Ruscitto, D. M., Wallace, P. J., Johnson, E. R., Kent, A. J. R., & Bindeman, I. N. (2010). Volatile contents of mafic magmas from cinder cones in the Central Oregon High Cascades: Implications for magma formation and mantle conditions in a hot arc. *Earth and Planetary Science Letters*, *298*(1-2), 153-161.

Ruscitto, D. M., Wallace, P. J., & Kent, A. J. R. (2011). Revisiting the compositions and volatile contents of olivine-hosted melt inclusions from the Mount Shasta region: implications for the formation of high-Mg andesites. *Contributions to Mineralogy and Petrology*, *162*(1), 109-132.

Ruth, D. C., Cottrell, E., Cortes, J. A., Kelley, K. A., & Calder, E. S. (2016). From passive degassing to violent strombolian eruptions: the case of the 2008 eruption of Llaima volcano, Chile. *Journal of Petrology*, *57*(9), 1833-1864.

Saal, A.E., Hauri, E.H., Langmuir, C.H., & Perfit, M.R. Vapour undersaturation in primitive mid-ocean-ridge basalt and the volatile content of Earth's upper mantle. *Nature* **419**, 451-455 (2002).

Saito, G., Morishita, Y., & Shinohara, H. (2010). Magma plumbing system of the 2000 eruption of Miyakejima volcano, Japan, deduced from volatile and major component contents of olivine-hosted melt inclusions. *Journal of Geophysical Research: Solid Earth*, *115*(B11).

Scaillet, B., Pichavant, M., & Roux, J. (1995). Experimental crystallization of leucogranite magmas. *Journal of Petrology*, *36*(3), 663-705.

Scaillet, B., Holtz, F., & Pichavant, M. (1997). Rheological properties of granitic magmas in their crystallization range. In *Granite: From segregation of melt to emplacement fabrics* (pp. 11-29). Springer, Dordrecht.

Scaillet, B. & Evans, B.W. The 15 June 1991 eruption of Mount Pinatubo. I. Phase equilibria and pre-eruption P-T-fO_2-fH_2O conditions of the dacite magma. *J. Petrol*. **40**, 381-411 (1999).

Scaillet, B., & Macdonald, R. A. Y. (2001). Phase relations of peralkaline silicic magmas and petrogenetic implications. *Journal of Petrology*, *42*(4), 825-845.

Scaillet, B., & Macdonald, R. (2006). Experimental constraints on pre-eruption conditions of pantelleritic magmas: evidence from the Eburru complex, Kenya Rift. *Lithos*, *91*(1-4), 95-108.

Scaillet, B. & Pichavant, M. Experimental constraints on volatile abundances in arc magmas and their implications fro degassing processes, in Volcanic degassing, C. Oppenheimer, D. Pyle & J. Barclay (eds.) *Geol. Soc. Spec. Pub*. 213, 23-52 (2003).

Scaillet, B., Clemente, B., Evans, B.W., Pichavant, M. Redox control of sulfur degassing in silicic magmas. *J. Geophys. Res.* **103**, 23937-23949 (1998).

Scaillet, B., Holtz, F., & Pichavant, M. (2016). Experimental constraints on the formation of silicic magmas. *Elements*, *12*(2), 109-114.

Schmidt, M.W . & Poli, S. Experimentally based water budgets for dehydrating slabs and consequences for arc magma generation. *Earth Planet. Sci. Lett.* **163,** 361-379 (1998).

Shaw, A. M., Behn, M. D., Humphris, S. E., Sohn, R. A., & Gregg, P. M. (2010). Deep pooling of low degree melts and volatile fluxes at the 85 E segment of the Gakkel Ridge: evidence from olivine-hosted melt inclusions and glasses. *Earth and Planetary Science Letters*, *289*(3-4), 311-322.

Sisson, T. W. & Bacon, C.R. Gas-driven filter pressing in magmas. *Geology* **27**, 613-616 (1999).

Sisson, T. W., & Bronto, S. (1998). Evidence for pressure-release melting beneath magmatic arcs from basalt at Galunggung, Indonesia. *Nature*, *391*(6670), 883-886.

Sisson, T. W., & Grove, T. L. (1993). Experimental investigations of the role of H_2O in calc-alkaline differentiation and subduction zone magmatism. *Contributions to Mineralogy and Petrology*, *113*(2), 143-166.

Sisson, T. W., Ratajeski, K., Hankins, W. B., & Glazner, A. F. (2005). Voluminous granitic magmas from common basaltic sources. *Contributions to Mineralogy and Petrology*, *148*(6), 635-661.

Spilliaert, N., Allard, P., Métrich, N., & Sobolev, A. V. (2006). Melt inclusion record of the conditions of ascent, degassing, and extrusion of volatile-rich alkali basalt during the powerful 2002 flank eruption of Mount Etna (Italy). *Journal of Geophysical Research: Solid Earth*, *111*(B4).

Stolper, E.M., Fine, G.J., Johnson, T., & Newman, S. The solubility of carbon dioxide in albitic melt. *Am. Mineral.* **72,** 1071–1085 (1987).

Syracuse, E. M., van Keken, P. E., & Abers, G. A. (2010). The global range of subduction zone thermal models. *Physics of the Earth and Planetary Interiors*, *183*(1-2), 73-90.

Tamic N., Behrens H., & Holtz F. The solubility of H_2O and CO_2 in rhyolitic melts in equilibrium with a mixed CO_2–H_2O fluid phase. *Chem. Geol.* **174,** 333–347,(2001).

Thomas, N., Tait, S. & Koyaguchi, T. Mixing of stratified liquids by the motion of gas bubbles : application to magma mixing. *Earth Planet. Sci. Lett.* **115**, 161-175 (1993).

Turner, S. J., & Langmuir, C. H. (2015). The global chemical systematics of arc front stratovolcanoes: Evaluating the role of crustal processes. *Earth and Planetary Science Letters*, *422*, 182-193.

Vielzeuf, D., & Montel, J. M. (1994). Partial melting of metagreywackes. Part I. Fluid-absent experiments and phase relationships. *Contributions to Mineralogy and Petrology*, *117*(4), 375-393.

Vielzeuf, D., & Schmidt, M. W. (2001). Melting relations in hydrous systems revisited: application to metapelites, metagreywackes and metabasalts. *Contributions to Mineralogy and Petrology*, *141*(3), 251.

Vigneresse, J.L., Barbey, P. & Cuney, M. Rheological transitions during partial melting and crystallisation with application to felsic magma segregation. *J. Petrol* **37**, 1579-1600 (1996).

Vigouroux, N., Wallace, P. J., & Kent, A. J. (2008). Volatiles in high-K magmas from the western Trans-Mexican Volcanic Belt: evidence for fluid fluxing and extreme enrichment of the mantle wedge by subduction processes. *Journal of Petrology*, *49*(9), 1589-1618.

Vigouroux, N., Wallace, P. J., Williams-Jones, G., Kelley, K., Kent, A. J., & Williams-Jones, A. E. (2012). The sources of volatile and fluid-mobile elements in the Sunda arc: A melt inclusion study from Kawah Ijen and Tambora volcanoes, Indonesia. *Geochemistry, Geophysics, Geosystems*, *13*(9).

Wallace, P. J. (2002). Volatiles in submarine basaltic glasses from the Northern Kerguelen Plateau (ODP Site 1140): Implications for source region compositions, magmatic processes, and plateau subsidence. *Journal of Petrology*, *43*(7), 1311-1326.

Wallace, P. Volatiles in subduction zone magmas: concentrations and fluxes based on melt inclusion and volcanic gas data. *J. Volc. Geoth. Res*. **140**, 217-240 (2005)

Wallace, P., Anderson, A.T. & Davis, A.M. Quantification of pre-eruptive exsolved gas contents in silicic magmas. *Nature* 377, 612-616 (1995).

Wallace, P. J., Anderson Jr, A. T., & Davis, A. M. (1999). Gradients in H2O, CO2, and exsolved gas in a large-volume silicic magma system: Interpreting the record preserved in melt inclusions from the Bishop Tuff. *Journal of Geophysical Research: Solid Earth*, *104*(B9), 20097-20122.

Wallace, P. J., Plank, T., Bodnar, R. J., Gaetani, G. A., & Shea, T. (2021). Olivine-hosted melt inclusions: a microscopic perspective on a complex magmatic world. *Annual Review of Earth and Planetary Sciences*, *49*.

Walowski, K.J., Wallace, P.J., Clynne, M.A., Rasmussen, D.J., and Weis, D., 2016, Slab melting and magma formation beneath the southern Cascade arc: Earth and Planetary Science Letters, v. 446, p. 100–112.

Wanless, V. D., Shaw, A. M., Behn, M. D., Soule, S. A., Escartín, J., & Hamelin, C. (2015). Magmatic plumbing at Lucky Strike volcano based on olivine-hosted melt inclusion compositions. *Geochemistry, Geophysics, Geosystems*, *16*(1), 126-147.

Watson, E.B. (1994). Diffusion in volatile-bearing magmas. In Carroll, M.R. & Holloway, J.R (eds), Volatiles in magmas. *Rev. Mineral*. 30, 371-412.

Webster, J. D., Taylor, B. E., & Bean, C. (1993). Pre-eruptive melt composition and constraints on degassing of a water-rich pantellerite magma, Fantale volcano, Ethiopia. *Contributions to Mineralogy and Petrology*, *114*(1), 53-62.

Wehrmann, H., Hoernle, K., Portnyagin, M., Wiedenbeck, M., & Heydolph, K. (2011). Volcanic CO_2 output at the Central American subduction zone inferred from melt inclusions in olivine crystals from mafic tephras. *Geochemistry, Geophysics, Geosystems*, *12*(6).

White, S. M., Crisp, J. A., & Spera, F. J. (2006). Long-term volumetric eruption rates and magma budgets. *Geochemistry, Geophysics, Geosystems*, *7*(3).

Wilding, M. C., Macdonald, R., Davies, J. E., & Fallick, A. E. (1993). Volatile characteristics of peralkaline rhyolites from Kenya: an ion microprobe, infrared spectroscopic and hydrogen isotope study. *Contributions to Mineralogy and Petrology*, *114*(2), 264-275.

Workman, R. K., Hauri, E., Hart, S. R., Wang, J., & Blusztajn, J. (2006). Volatile and trace elements in basaltic glasses from Samoa: Implications for water distribution in the mantle. *Earth and Planetary Science Letters*, *241*(3-4), 932-951.

Young, S.R. et al. Monitoring SO_2 emission at the Soufrière Hills volcano : implications for changes in eruptive conditions. *Geophys. Res. Lett.* **25,** 3681-3684 (1998)

Yoshimura, S., & Nakamura, M. (2011). Carbon dioxide transport in crustal magmatic systems. *Earth and Planetary Science Letters*, *307*(3-4), 470-478.

Yoshimura, S., & Nakamura, M. (2013). Flux of volcanic CO2 emission estimated from melt inclusions and fluid transport modelling. *Earth and Planetary Science Letters*, *361*, 497-503.

Zandt, G., Gilbert, H., Owens, T. J., Ducea, M., Saleeby, J., & Jones, C. H. (2004). Active foundering of a continental arc root beneath the southern Sierra Nevada in California. *Nature*, *431*(7004), 41-46.

Zhang, Y. (1999). H2O in rhyolitic glasses and melts: measurement, speciation, solubility, and diffusion. *Reviews of Geophysics*, *37*(4), 493-516.

Zhang, Y., Xu, Z., Zhu, M., & Wang, H. (2007). Silicate melt properties and volcanic eruptions. *Reviews of Geophysics*, *45*(4).

Zimmer, M. M., Plank, T., Hauri, E. H., Yogodzinski, G. M., Stelling, P., Larsen, J., ... & Nye, C. J. (2010). The role of water in generating the calc-alkaline trend: new volatile data for Aleutian magmas and a new tholeiitic index. *Journal of Petrology*, *51*(12), 2411-2444.

Legend of figures

Figure 1 : T-XH_2O_{fluid} position of solidus (100% crystals) and 1 % crystal proportion curves, for andesite, dacite, rhyolite and high silica rhyolite (HSR) compositions, as constrained from phase equilibrium data. At any given temperature, experimental data show that melt fraction varies nearly linearly with H_2O dissolved in melt. Relative to arrow A, an influx of mafic gas may induce melting if $XH_2O_{fluid} > 0.8$ (ex arrow C), or crystallisation for $XH_2O_{fluid} < 0.8$ (ex arrow B). A fluid having a composition of arrow D will drive the system toward full crystallisation. For a fixed temperature, the range of melt H_2O content between H_2O-saturation and solidus is strongly dependent on the bulk composition. At 700°C, HSR, for instance, displays a very narrow interval in H_2O melt content, which implies that HSR are more sensitive to mafic fluid influx than are more mafic compositions. All magmas share approximately the same solidus, which is taken as that of the haplogranite system, a consequence of the fact that in typical arc magmas the residual liquid almost always trend toward high silica rhyolite composition. Note that the range of melt water contents between solidus and water saturation increases with temperature: for instance at 700°C it ranges from 7 wt% to 5 wt%, while at 800°C, it ranges from 7 wt% down to 2.5 wt%.

Figure 2 : Relationship between ascent rate of bubble and its radius in a magma having a residual melt with a viscosity of $10^{4.5}$ Pa s and a crystal load of 0, 50 and 70 %, which encompass storage conditions of andesitic to rhyolite arc magmas. The solid lines are calculations for a fluid density of 500 kg/m^3 (i.e. at around 2 kbar), while those dashed are for a fluid density of 1000 kg/m^3 (10 kbar).

Figure 3. Evolution of magma crystallinity and temperature with addition of fluid for the case of silicic compositions. A, B, Haplogranite at 200 MPa (Johannes and Holtz, 2012), with starting conditions prior to fluid infiltration being 700°C and 4 wt% dissolved H_2O. Trends are calculated for various fluid compositions (XH_2O_{fluid}). Note the rapid change upon the addition of the first 5 wt% fluid. In this case, temperature changes remain modest. C, D Rhyolite at 200 MPa with starting conditions prior to fluid infiltration being 700°C and 6 wt% dissolved H_2O. In this case, complete solidification of the rhyolite occurs with infiltration of 35 wt% fluid with XH_2O_{fluid}=0.4, and is accompagnied by a temperature increase of about 70°C. E,F panels are for the same rhyolite but at 400 MPa. See text for more explanations.

Figure 4. Evolution of magma crystallinity and temperature with addition of fluid for the case of a dacite composition at three different pressures. A, B, at 220 MPa ; C,D at 390 MPa, and E,F at 960 MPa. Trends are calculated for various fluid compositions (XH_2O_{fluid}). Note the significant decrease in melt fraction at 960 MPa for XH_2O_{fluid} = 0.7 and 0.9, as compared to the moderate effect of similar fluid compositions at 220 MPa. See text for explanations.

Figure 5. Evolution of magma crystallinity and temperature with addition of fluid for the case of an andesite composition at two different pressures. A, B, at 220 MPa ; C,D at 400 MPa.

Trends are calculated for various fluid compositions (XH_2O_{fluid}) with T-H_2O content corresponding to pre-eruptive conditions inferred for Mt Pelée and Montserrat volcanoes. Note that small amounts of fluid (<5 wt%) are required to produce significant changes in magma crystallinity, shifting the system accross the rheological threshold of magma mobility (ca 50 wt% crystals). See text for explanations.

Figure 6. Evolution of magma crystallinity and temperature with addition of fluid for the case of a basaltic-andesite composition at lower crustal pressures. A, B, at 800 MPa ; C, D at 1200 MPa. Trends are calculated for various fluid compositions (XH_2O_{fluid}) and two different initial temperatures-H_2O. Note that even the driest fluids (XH_2O_{fluid} =0.1) produce a very small increase in magma crystallinity, in contrast to what happens at upper crustal pressures. See text for explanations.

Figure 7. Evolution of magma crystallinity and temperature with addition of fluid for the case of a basaltic composition at mid to upper crustal pressures. A, B, at 200 MPa ; C,D at 500 MPa, and E,F at 400 MPa for the Stromboli composition. Trends are calculated for various fluid compositions (XH_2O_{fluid}) and different initial temperatures-H_2O, selected to encompass those inferred for some near liquidus primitive arc basalt. See text for explanations.

Figure 8 : Relationships between XH_2O_{fluid} and pressure, calculated for various fH_2O and temperatures, selected to be representative of T-H_2O conditions of arc magmas. Calculations have been made for the following fH_2O : 1480 bar (corresponding to ca 6 wt% H_2O in silicic melts, or 5 wt% in mafic ones), 1000 bar (4 wt%), 500 bar (2 wt%). For a magma with a given dissolved H_2O (or fH_2O), the equilibrium XH_2O_{fluid} can obtained if the pressure of storage is known. Infiltration of such a magma by a fluid having a lower XH_2O_{fluid} than this

equilibrium value will lead to crystallisation. Conversely, if the infiltrating fluid has a higher XH_2O_{fluid}, it will lead to melting. Because many silicic to intermediate arc magmas are stored at *ca* 2 kb with an equilibrium XH_2O_{fluid}>0.8, their infiltration by CO_2 bearing fluids emanating from underlying basalts is more likely to induce crystallisation than melting. Red circles represent silicic to andesitic arc magmas for which phase equilibrium data are available for their pre-eruptive conditions (Scaillet & Pichavant, 2003). Green dots correspond to pre-eruption conditions of felsic reservoirs in hot-spot and ridge settings. Note the unique position of the Erebus system, in the left part of the diagram. Sources for the different categories of basalts are given in the main text the sources of data are:

Arc: Spillaert et al., (2006) (Etna), Métrich et al. (2010) (Stromboli) ; Bertagnini et al. (2003) (Stromboli) ; Johnson et al. (2009) (Mexican) Saito et al. (2010) (Miakejima), Marianelli et al. (1999,2005) (Vesuvius), Roggensack et al. (1997) (Cerro Negro) ; Sisson and Bronto (1998) Galunggung); Cervantes and Wallace (2003) (Chichinautzin); Luhr (2001) (Paricutin); Roggensack (2001)(Fuego), Zimmer et al. (2010)(Aleutians-Alaska); Ruscitto et al. (2010) (Oregon); Ruscitto et al. (2011)(Shasta); Ruth et al. (2016)(Llaima); Wehrmann et al. (2011),(Central America); Walowski et al. (2015); Vigouroux et al. (2012)(Sunda arc); Vigouroux et al. (2008)(Trans-Mexican) ; Brounce et al. (2014)(Mariana arc) ; Johnson et al. (2008)(Jorullo) ; Kelley et al. (2010)(Mariana Arc); Le Voyer et al. (2010)(Shasta); Lloyd et al. (2014)(Fuego) ; Métrich et al. (2011)(Siwi) ; Maria and Luhr (2000)(Mexican) ; Moretti et al. (2013)(Ischia); Nichols et al. (2012)(Izu); Plechov et al. (2015)(Tolbachik); Robidoux et al. (2017)(San Cristobal);

Hot Spot: Dixon et al., (1991) (Kilauea) ; Bureau et al. (1998, 1999) (Réunion) ; Métrich and Clocchiatti (1996)(Réunion) ; Dixon et al. (1997) (Hawaii) ; Wallace (2002) (Kerguelen) ; Borisova et al. (2002) (Kerguelen) ; Dixon and Clague (2001)(Loihi); Workman et al (2006)(Samoa); Hauri (2002)(Hawaii); Anderson and Brown (1993)(Hawaii); Colman et

al. (2015)(Galapagos); Davis et al. (2003)(Mauna Loa); Cabral et al. (2014)(Mangaia) ; Di Muro et al. (2014)(Réunion) ; Jackson et al. (2015)(Tuvalu) ; Jackson et al. (2015)(Ontong Java) ; Koleszar et al. (2009)(Galapagos) ; Longpre et al. (2016)(El Hierro) ; Métrich et al. (2014)(Azores) ; Pietruszka et al. (2011)(Loihi)

Rift/ridges: Head et al. 2010 (Nyamuragira) ; Wanless et al. (2015)(Lucky Strike) ; Saal et al. (2002)(Siqueiros); Shaw et al. (2010)(Gakkel); Le Voyer et al. (2015)(MORB); Helo et al. (2011)(Juan de Fuca ridge).

Table 1. Magma compositions used fo simulations

	Haplogranite	Rhyolite AB422	Rhyolite DK89	Dacite Pinatubo	Andesite Mt Pelée/D29	Andesite Huerto	Basaltic Andesite	MOIB1	Alkali basalt 0B93-190	Basalt Stromboli
Pressure (MPa)	200	200	400	200/390/960	200	400	800/1200	200	500	400
SiO_2	76.14	73.61	73.48	65.57	62.20	62.79	58.19	49.56	48.84	50.61
TiO_2	-	0.38	0.13	0.45	0.50	0.82	0.97	0.83	2.75	0.81
Al_2O_3	13.53	13.28	15.41	16.37	17.49	16.62	19.16	16.32	16.14	15.24
FeO_{tot}	-	2.54	0.91	4.50	6.39	6.07	6.31	8.70	11.85	7.89
MnO	-	0.05	0.01	0.14	0.14	0.08	0.31	0.16	0.17	0.10
MgO	-	0.49	0.20	2.11	2.28	1.96	3.00	9.73	5.86	8.19
CaO	-	1.33	0.86	4.82	6.35	5.31	7.56	12.33	9.76	12.30
Na_2O	4.65	3.37	3.87	4.45	3.59	3.55	3.00	2.16	3.12	2.36
K_2O	5.68	4.95	4.99	1.58	1.06	2.52	1.51	0.07	1.12	1.87
P_2O_5	-	-	0.14	-	-	0.29	-	0.09	0.40	0.63
Total	100	100	100	100	100	100	100	100	100	100

Haplogranite :Johannes and Holtz (2012), Metaluminous rhyolite : Klimm et al., 2003 ; Peraluminous rhyolite :Scaillet et al., 1995 ; Dacite Pinatubo : Scaillet and Evans, 1999 ; Andesite Mt Pelée : Martel et al., 1999 ; Andesite Huerto :Parat et al., 2008 ; Basaltic andesite : Alonso Perez et al., 2009 ; MORB : Berndt et al., 2005 ; Alkali basalt : Freise et al., 2009 ; Stromboli basalt : Di Carlo et al., 2006.

Table 2. Coefficients for calculating melt fraction with T and H_2O_{melt}[1]

Composition	Pressure (MPa)	a	b	c	d
Haplogranite	200	135.93	-0.0464	33.151	0.2181
Rhyolite	200	-0.2589	232.24	1.6569	-388.4
Rhyolite	400	0.2200	-130.37	-1.8962	1231.8
Dacite	200	-0.1176	116.264	1.0751	-952.8
Dacite	390	0.0287	-11.372	0.1076	-21.77
Dacite	960	-0.0642	67.085	0.8837	-95.85
Andesite	200	0.1197	-94.136	-0.4301	359.82
Andesite	400	-0.0794	82.267	0.7901	-

Basaltic-andesite	800	-0.0098	9.6127	0.3734	01.72 -
Basaltic-andesite	1200	-0.1033	104.895	1.3599	74.76 -
Basalt	200	-0.1009	124.28	0.8952	274.54 -
Basalt	500	-0.0373	42.72	0.6882	51.78 -
Basalt	400	0.0640	-58.944	0.1555	57.32 - 34.57

[1]T in °C and H_2O_{melt} in wt%

Table 3. Coefficients for calculating H_2O contents of melts from f_{H2O}

Composition	Pressure (MPa)	*e*	*f*	Type of equation[1]
Haplogranite	200	0.1250	0.5297	$e f_{H2O}^{f}$
Rhyolite	200	0.0009	1.2530	f_{H2O}
Rhyolite	400	0.1618	0.4912	$e f_{H2O}^{f}$
Dacite	200	0.3859	0.3869	$e f_{H2O}^{f}$
Dacite	390	0.3859	0.3869	$e f_{H2O}^{f}$
Dacite	960	2.1414	-8.6388	$e \ln f_{H2O} + f$
Andesite	200	0.1007	0.5954	$e f_{H2O}^{f}$
Andesite	400	0.2196	0.4469	$e f_{H2O}^{f}$
Basaltic-andesite	800	0.0008	5.964	$e f_{H2O} + f$
Basaltic-andesite	1200	0.0008	5.964	$e f_{H2O} + f$

[1]H_2O in wt% and fH_2O in MPa

Table 4. Thermal parameters

$C_{p\ liquid}$[1], J g^{-1} K^{-1}	1.4
$C_{p\ solid}$[1], J g^{-1} K^{-1}	1.3
$C_{p\text{-}H2O}$[2], J g^{-1} K^{-1}	3.9
$C_{p\text{-}CO2}$[2], J g^{-1} K^{-1}	1.4
L_{felsic}[1], J g^{-1}	270
L_{mafic}[1], J g^{-1}	400

[1]Bachman and Bergantz (2003)
[2] Labotka (1991)

Declaration of interests

☐The authors declare that they have no known competing financial interests or personal relationships that could have appeared to influence the work reported in this paper.

☒The authors declare the following financial interests/personal relationships which may be considered as potential competing interests:

Scaillet Bruno reports financial support was provided by National Centre for Scientific Research. Scaillet Bruno reports financial support was provided by French National Research Agency. Scaillet Bruno has patent pending to none. none

- Long term fluxing of felsic to intermediate magma bodies stored in upper crust by mafic volatiles generally lead to their isothermal solidification.
- Conversely, for bodies stagnating in the mid to deep crust, such a process almost inevitably enhances melting, driving or maintaining magmas beyond the threshold of mobility needed for upward material transfer, unless the percolating fluid is very CO_2-rich
- Crustal growth may thus be in part limited by the difficulty of crystallising deep-seated magma bodies, in particular in arc settings.

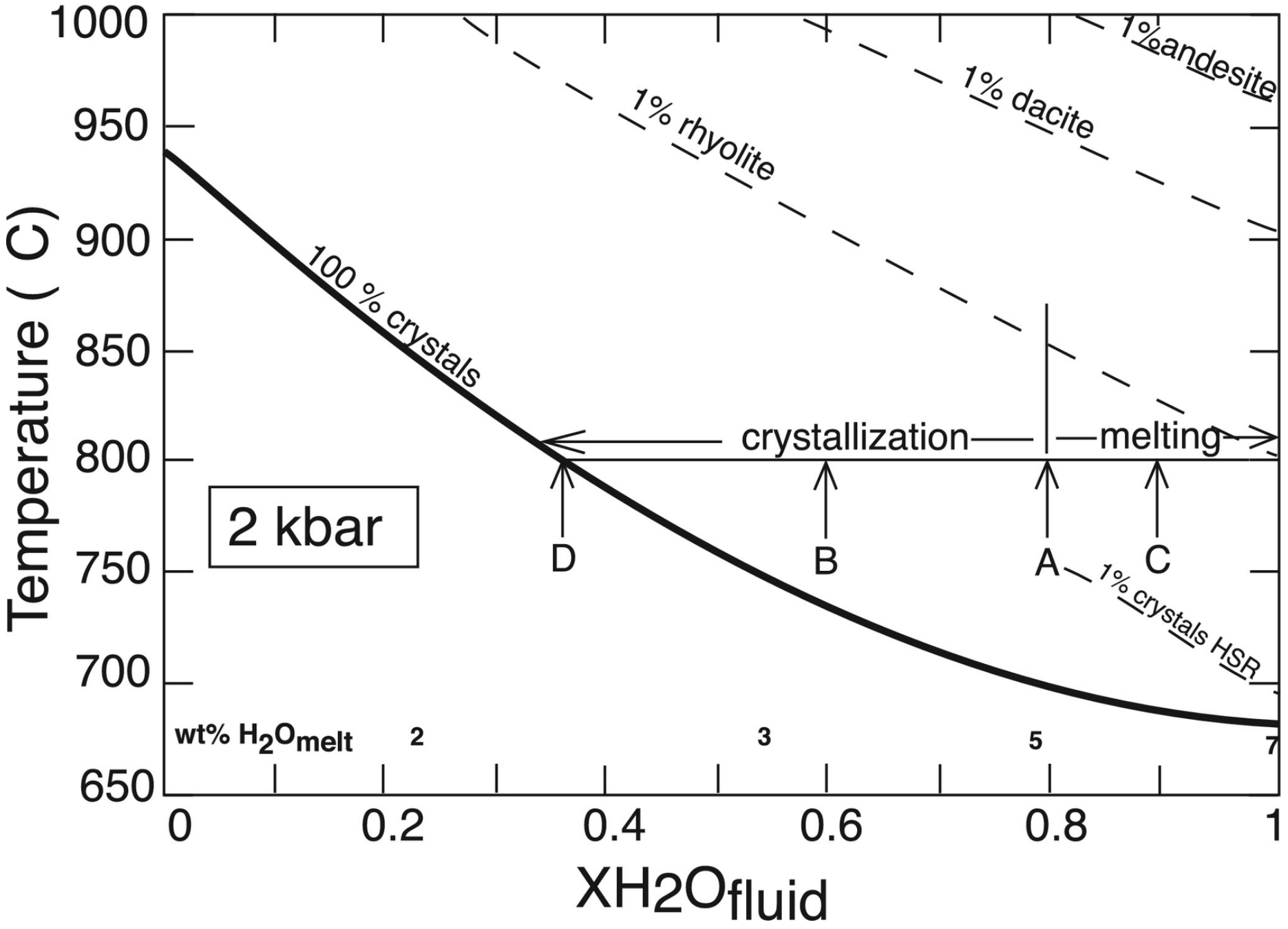
1000
950
900
850
800
750
700
650
Temperature (C)
0
0.2
0.4
0.6
0.8
1
XH2Ofluid
1% andesite
1% dacite
1% rhyolite
100 % crystals
crystallization
melting
2 kbar
D
B
A
C
1% crystals HSR
wt% H2Omelt
2
3
5
7

Figure 1

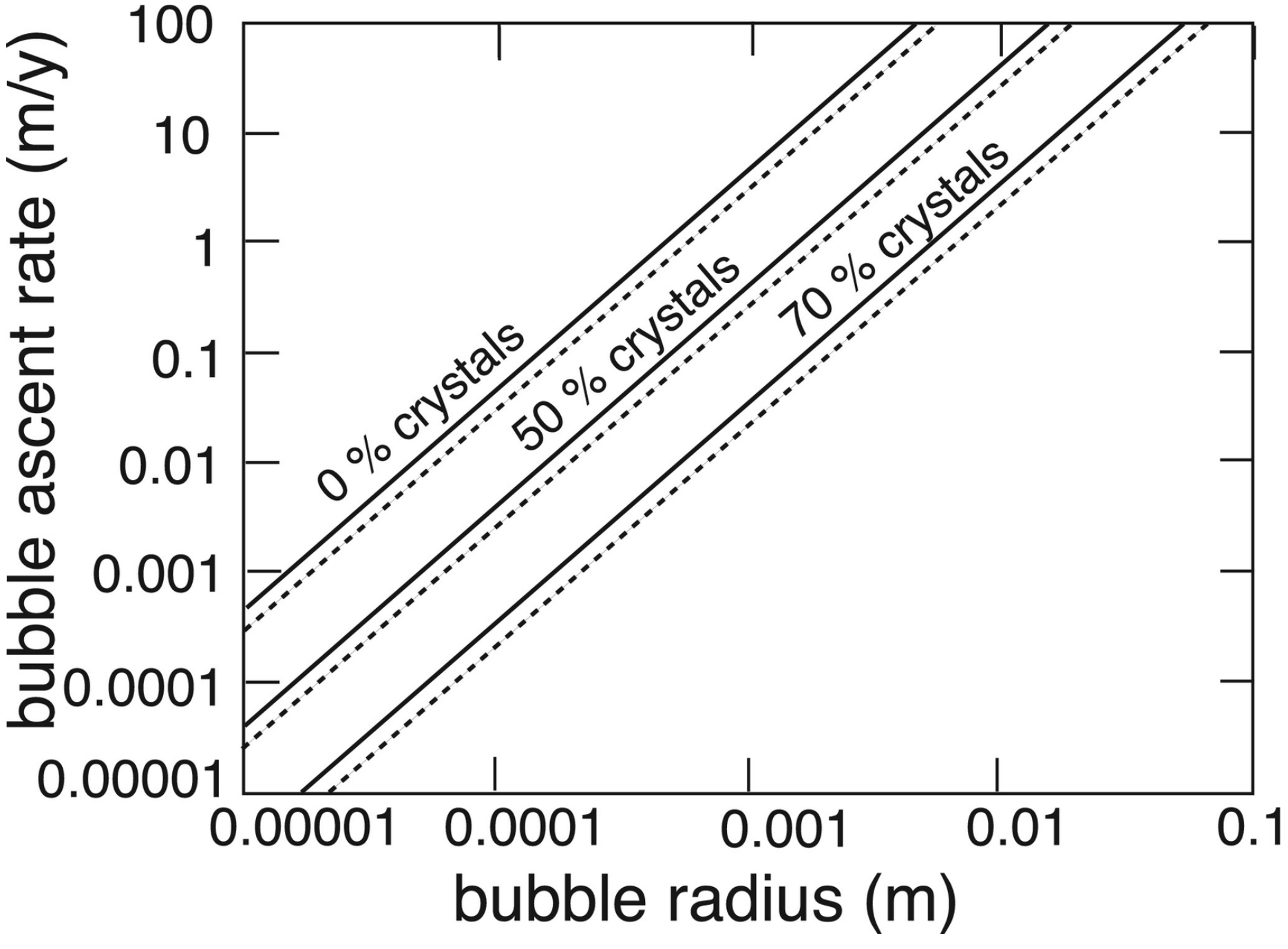
100
10
1
0.1
0.01
0.001
0.0001
0.00001
bubble ascent rate (m/y)
0.00001
0.0001
0.001
0.01
0.1
bubble radius (m)
0 % crystals
50 % crystals
70 % crystals

Figure 2

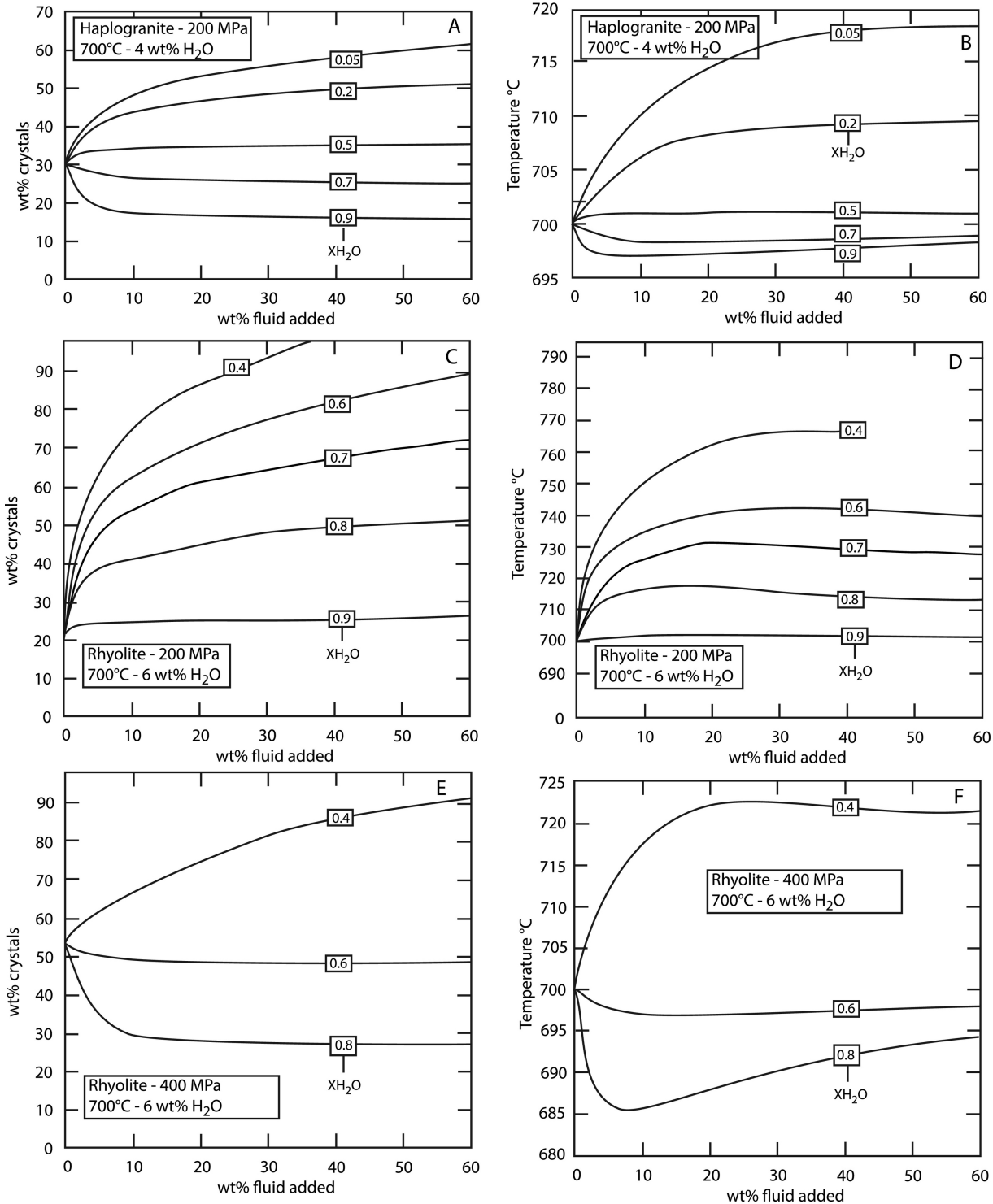
A
Haplogranite - 200 MPa
700°C - 4 wt% H2O
wt% crystals
wt% fluid added
0.05
0.2
0.5
0.7
0.9
XH2O
B
Haplogranite - 200 MPa
700°C - 4 wt% H2O
Temperature °C
wt% fluid added
0.05
0.2
0.5
0.7
0.9
XH2O
C
Rhyolite - 200 MPa
700°C - 6 wt% H2O
wt% crystals
wt% fluid added
0.4
0.6
0.7
0.8
0.9
XH2O
D
Rhyolite - 200 MPa
700°C - 6 wt% H2O
Temperature °C
wt% fluid added
0.4
0.6
0.7
0.8
0.9
XH2O
E
Rhyolite - 400 MPa
700°C - 6 wt% H2O
wt% crystals
wt% fluid added
0.4
0.6
0.8
XH2O
F
Rhyolite - 400 MPa
700°C - 6 wt% H2O
Temperature °C
wt% fluid added
0.4
0.6
0.8
XH2O

Figure 3

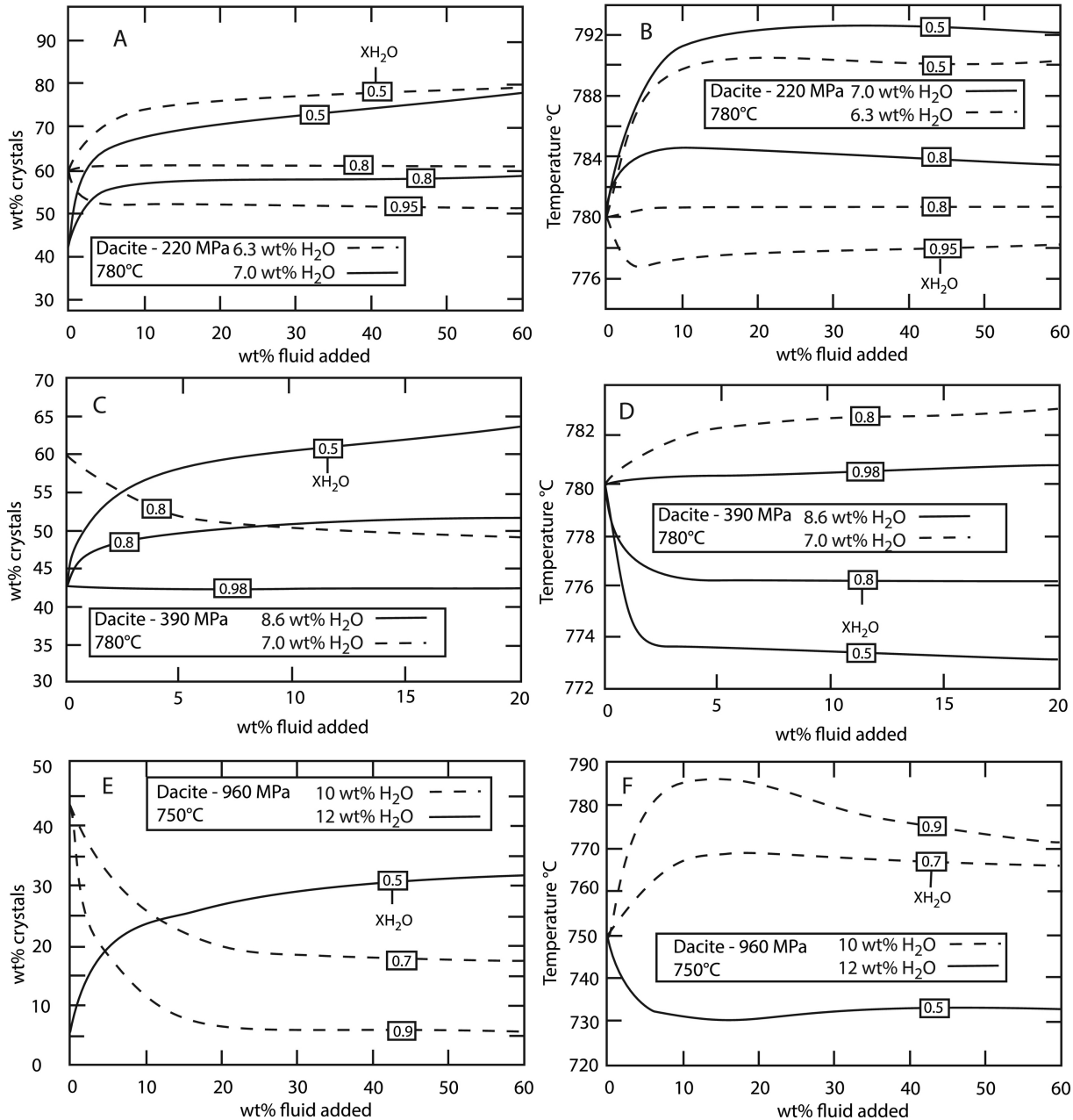
A
XH2O
0.5
0.5
0.8
0.8
0.95
Dacite - 220 MPa 6.3 wt% H2O
780°C 7.0 wt% H2O
wt% crystals
wt% fluid added
B
0.5
0.5
Dacite - 220 MPa 7.0 wt% H2O
780°C 6.3 wt% H2O
0.8
0.8
0.95
XH2O
Temperature °C
wt% fluid added
C
0.5
XH2O
0.8
0.8
0.98
Dacite - 390 MPa 8.6 wt% H2O
780°C 7.0 wt% H2O
wt% crystals
wt% fluid added
D
0.8
0.98
Dacite - 390 MPa 8.6 wt% H2O
780°C 7.0 wt% H2O
0.8
XH2O
0.5
Temperature °C
wt% fluid added
E
Dacite - 960 MPa 10 wt% H2O
750°C 12 wt% H2O
0.5
XH2O
0.7
0.9
wt% crystals
wt% fluid added
F
0.9
0.7
XH2O
Dacite - 960 MPa 10 wt% H2O
750°C 12 wt% H2O
0.5
Temperature °C
wt% fluid added

Figure 4

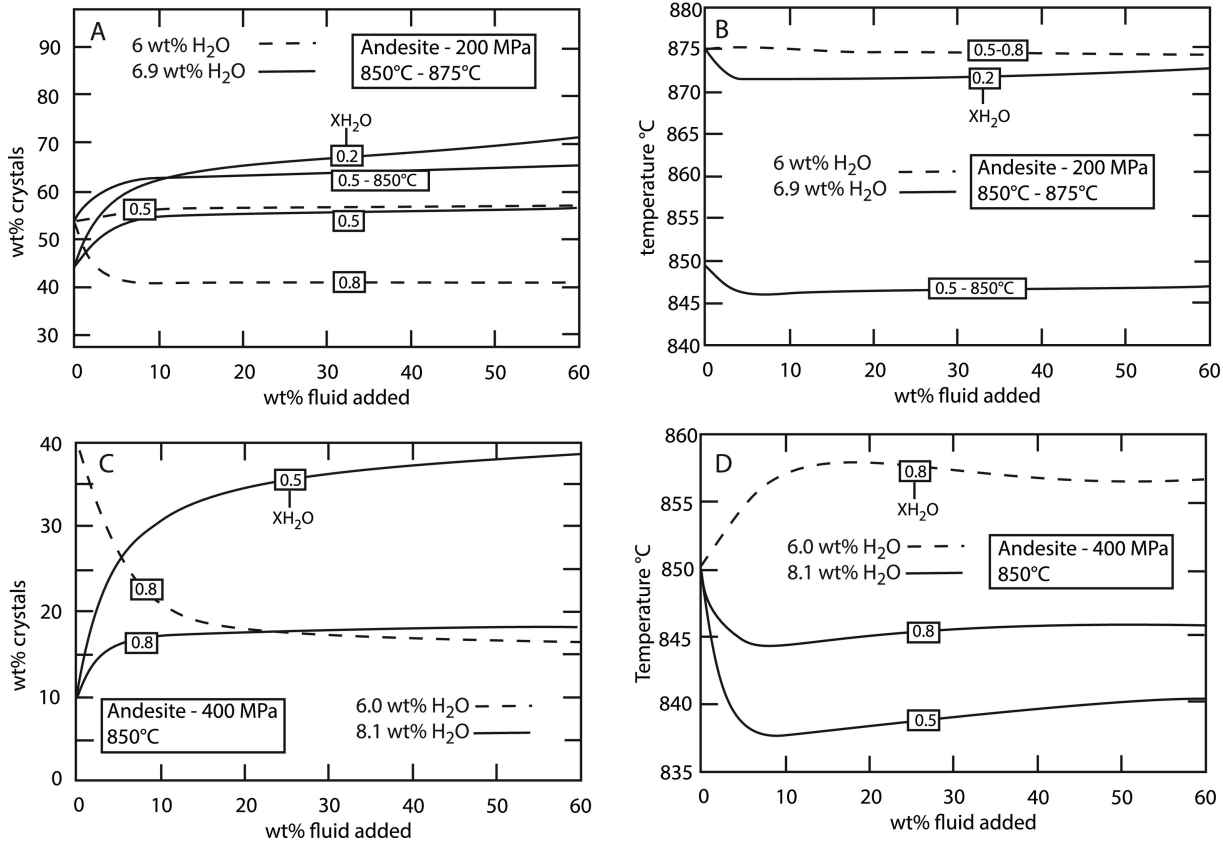
A
6 wt% H2O
6.9 wt% H2O
Andesite - 200 MPa
850°C - 875°C
XH2O
0.2
0.5 - 850°C
0.5
0.5
0.8
wt% crystals
wt% fluid added
B
0.5-0.8
0.2
XH2O
6 wt% H2O
6.9 wt% H2O
Andesite - 200 MPa
850°C - 875°C
0.5 - 850°C
temperature °C
wt% fluid added
C
0.5
XH2O
0.8
0.8
Andesite - 400 MPa
850°C
6.0 wt% H2O
8.1 wt% H2O
wt% crystals
wt% fluid added
D
0.8
XH2O
6.0 wt% H2O
8.1 wt% H2O
Andesite - 400 MPa
850°C
0.8
0.5
Temperature °C
wt% fluid added

Figure 5

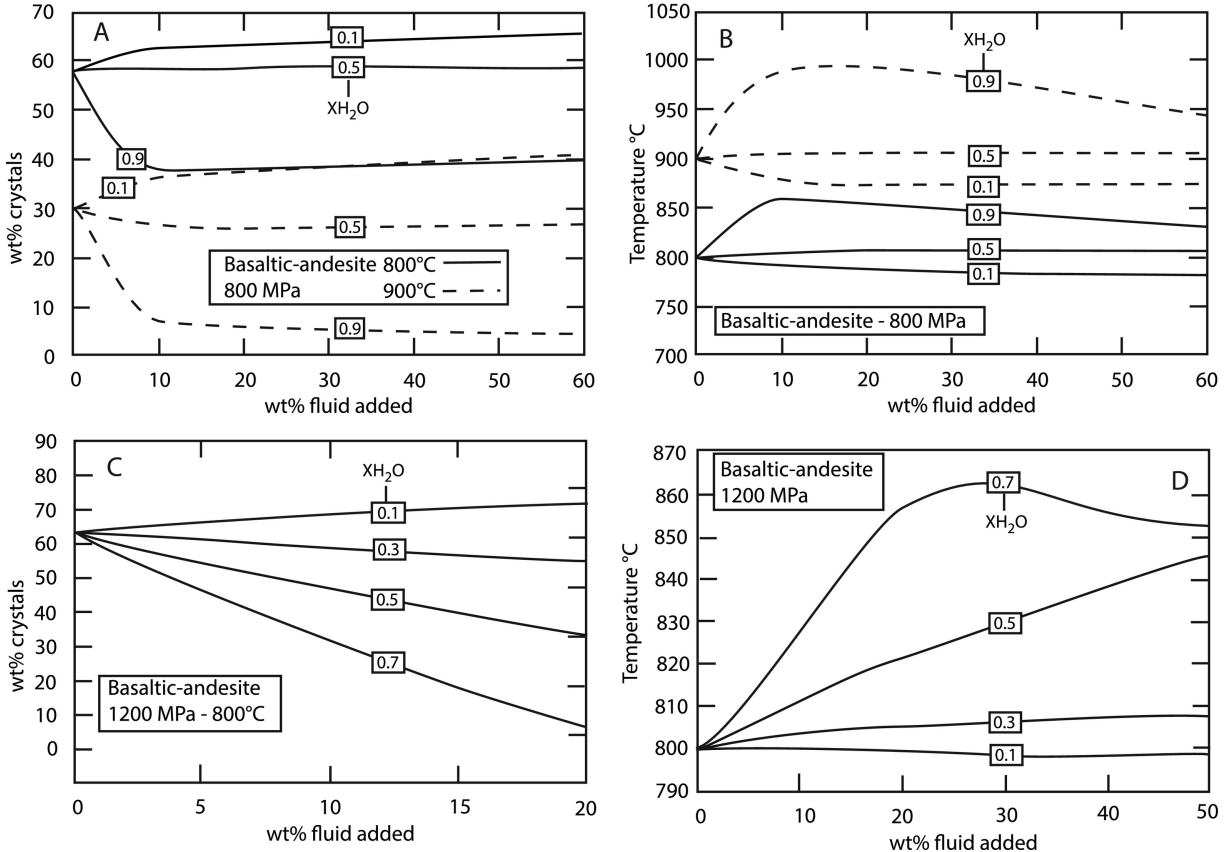
A
wt% crystals
wt% fluid added
XH2O
0.1
0.5
0.9
Basaltic-andesite 800°C
800 MPa
900°C
B
Temperature °C
wt% fluid added
XH2O
0.9
0.5
0.1
Basaltic-andesite - 800 MPa
C
wt% crystals
wt% fluid added
XH2O
0.1
0.3
0.5
0.7
Basaltic-andesite
1200 MPa - 800°C
D
Temperature °C
wt% fluid added
Basaltic-andesite
1200 MPa
0.7
XH2O
0.5
0.3
0.1

Figure 6

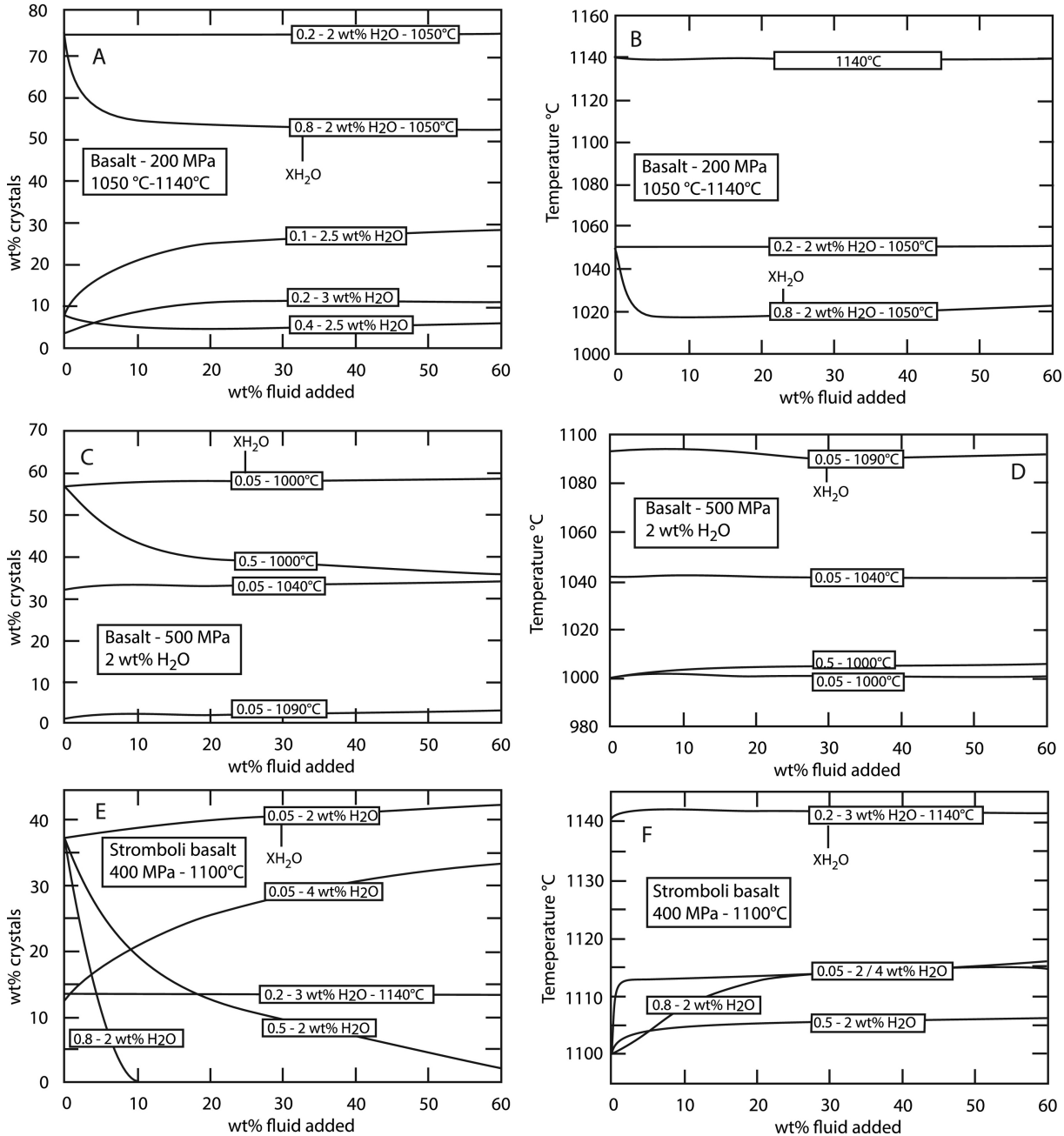
A
0.2 - 2 wt% H2O - 1050°C
0.8 - 2 wt% H2O - 1050°C
XH2O
Basalt - 200 MPa
1050 °C-1140°C
0.1 - 2.5 wt% H2O
0.2 - 3 wt% H2O
0.4 - 2.5 wt% H2O
wt% crystals
wt% fluid added
B
1140°C
Basalt - 200 MPa
1050 °C-1140°C
0.2 - 2 wt% H2O - 1050°C
XH2O
0.8 - 2 wt% H2O - 1050°C
Temperature °C
wt% fluid added
C
XH2O
0.05 - 1000°C
0.5 - 1000°C
0.05 - 1040°C
Basalt - 500 MPa
2 wt% H2O
0.05 - 1090°C
wt% crystals
wt% fluid added
D
0.05 - 1090°C
XH2O
Basalt - 500 MPa
2 wt% H2O
0.05 - 1040°C
0.5 - 1000°C
0.05 - 1000°C
Temperature °C
wt% fluid added
E
0.05 - 2 wt% H2O
XH2O
Stromboli basalt
400 MPa - 1100°C
0.05 - 4 wt% H2O
0.2 - 3 wt% H2O - 1140°C
0.5 - 2 wt% H2O
0.8 - 2 wt% H2O
wt% crystals
wt% fluid added
F
0.2 - 3 wt% H2O - 1140°C
XH2O
Stromboli basalt
400 MPa - 1100°C
0.05 - 2 / 4 wt% H2O
0.8 - 2 wt% H2O
0.5 - 2 wt% H2O
Temeperature °C
wt% fluid added

Figure 7

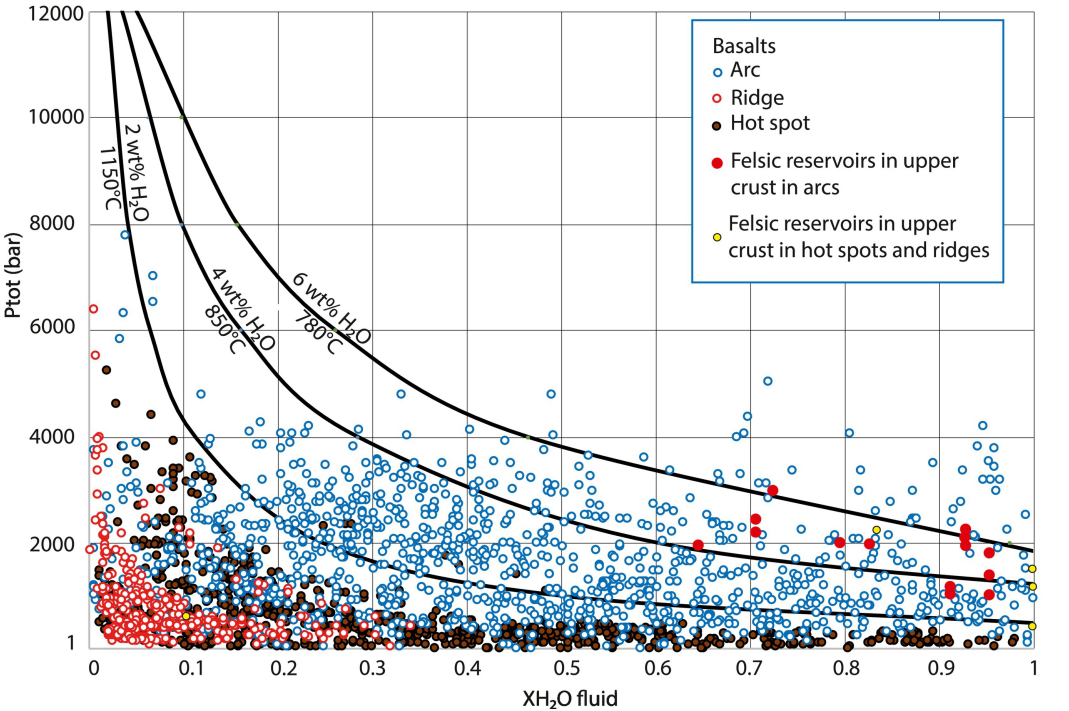
Basalts
Arc
Ridge
Hot spot
Felsic reservoirs in upper crust in arcs
Felsic reservoirs in upper crust in hot spots and ridges
2 wt% H2O
1150°C
4 wt% H2O
850°C
6 wt% H2O
780°C
Ptot (bar)
XH2O fluid
12000
10000
8000
6000
4000
2000
1
0
0.1
0.2
0.3
0.4
0.5
0.6
0.7
0.8
0.9
1

Figure 8